NASA
Technical
Paper
2475

C.2

June 1985

Correlation of Predicted and Measured Sonic Boom Characteristics From the Reentry of STS-1 Orbiter

Frank Garcia, Jr.,
Jess H. Jones, and
Herbert R. Henderson

NASA

Correlation of Predicted and Measured Sonic Boom Characteristics From the Reentry of STS-1 Orbiter

Frank Garcia, Jr.
Lyndon B. Johnson Space Center
Houston, Texas

Jess H. Jones
George C. Marshall Space Flight Center
Marshall Space Flight Center, Alabama

Herbert R. Henderson
Langley Research Center
Hampton, Virginia

CONTENTS

TABLES

FIGURES

ABSTRACT

An analysis correlating characteristics from 44 sonic boom pressure signatures recorded at 11 locations during the reentry of the Orbiter *Columbia* with wind tunnel signatures extrapolated from flight altitudes has been made for Mach numbers M ranging from 1.23 to 5.87. The flight pressure signatures were recorded by microphones positioned at ground level and simulated ear level near the descent groundtrack along the California corridor. The wind tunnel signatures used in the theoretical predictions were measured using a 0.0041-scale model Orbiter. The range of peak overpressures recorded at 11 stations during Orbiter descent was from 33.16 N/m^2 at $M = 5.87$ to 114.91 N/m^2 at $M = 1.76$. The mean difference between all measured overpressures and those predicted using wind tunnel signatures and trajectory characteristics inferred from flight data was 12 percent from the measured levels. With one exception, the flight signatures exhibited a shape very similar to theoretical N-waves; the $M = 5.87$ signature has a rounded peak as opposed to a sharp peak. This difference in shape is typical of flight signatures that are propagated from extremely high altitudes such as this one, which originated at 39 337 meters, and subjected to atmospheric turbulence.

INTRODUCTION

No fully theoretical methods are available for calculating the sonic boom overpressures generated by blunt vehicles with detached shock wave maneuvering at high Mach numbers and high angles of attack. Therefore, sonic boom estimates for the Space Shuttle Orbiter and similar vehicles must be based on one of the currently available semiempirical techniques (refs. 1 and 2). With these techniques, near-field pressure signatures measured in wind tunnels are extrapolated to the far field in a real atmosphere under actual flight conditions. To extend the range of conditions for which these techniques are valid, measurements were made in the early 1970's using the Apollo 15 and 16 command modules as test vehicles. Results from both of these flights are reported in references 3 to 5, and agreement between predicted and flight results was good. This agreement provided some level of confidence in the capability of semiempirical techniques to predict sonic boom overpressure levels during descent on blunt vehicles such as the Orbiter. These predicted levels currently are baselined as required by law in the Space Shuttle Program Environmental Impact Statement (ref. 6).

This report contains results of the flight pressure signatures recorded at 11 stations during the descent of the Orbiter *Columbia* including characteristics such as overpressure levels, wave duration, rise time, and corresponding frequency content. Signatures were recorded by microphones placed at ground level and simulated ear level under or near the Orbiter descent groundtrack along the California corridor from Mach numbers $M = 5.87$ to $M = 1.23$. These signatures are analyzed and their amplitudes and durations are then compared with estimates based on the wind tunnel data of references 7 and 8 and inferred postflight trajectory data using the extrapolation procedure of reference 1.

APPARATUS AND METHODS

Test Vehicle

A schematic of the STS-1 Orbiter *Columbia* (descent configuration) on which sonic boom levels were measured during entry is shown in figure 1. The Orbiter *Columbia* is a lifting vehicle capable of meaneuvering and landing much like an airplane by using its control surfaces, which are augmented by a reaction control system. As such, during atmospheric flight, it is capable of flying at angles of attack as high as 40° and rolling about the velocity vector to ±70°. Figure 2 is a photograph of the Orbiter *Columbia* in flight on its way to a landing at the Edwards Air Force Base (EAFB) dry lakebed in California, terminating the STS-1 mission. *Columbia* has an over-all length of 32.77 meters and had a gross weight at entry interface (121 920 meters altitude) of 90 720 kilograms during the STS-1 mission.

Test Area and Arrangement

The general test areas associated with the entry of the Orbiter *Columbia* during the STS-1 mission are shown in figure 3. To define these test areas, a preflight STS-1 sonic boom analysis was performed based on the final pre-flight predicted STS-1 Operational Flight Profile[1] for a nominal entry into EAFB. This analysis defined the theoretically desired locations for the 11 sonic boom stations shown in figure 3 by a circled number (0 to 10) and located near the entry groundtrack shown as a dashed line on the same fig-ure. The predicted overpressure levels at those locations were used to set the signal-conditioning amplifiers at each station.

Selection of the recommended measurement station locations was based on several considerations. Since the primary objective of the sonic boom measurement program is to verify the theoretical technique used to predict sonic boom overpressures (ref. 1), the station locations were distributed across the flight Mach number range for which wind-tunnel-measured pressure signatures exist to verify the data base. Consequently, the layout of the measurement stations on this flight was designed primarily to confirm the longitudinal trend of overpressure level with Mach number and secondarily, the lateral trend of overpressure with Mach number in the area of expected high overpressures. Most of the station locations were selected to capture pressure signatures in the region of maximum predicted overpressure level, which occurs in the immediate vicinity of the EAFB lakebed. This selection criterion also has the advantage of locating the measurement stations in the part of the entry groundtrack least affected by atmosphere and trajectory dispersions.

---

[1]STS-1 Operational Flight Profile, Volume V, Descent - Cycle 3.2.3. NASA Lyndon B. Johnson Space Center Mission Planning and Analysis Division rep. JSC-16916, Mar. 1981.

The actual final locations for the 11 measurement stations are listed in table I. Shown are the lateral distance by which each station is perpendicularly offset from the ground-projected flightpath and the station position and elevation.

Spacecraft Positioning

The STS-1 Orbiter *Columbia* was launched from the NASA John F. Kennedy Space Center, Florida, on April 12, 1981, at an inclination of 40.3°. The mission had a duration of 2-1/2 days, and the Orbiter *Columbia* reentered the Earth's atmosphere over the mid-Pacific Ocean between Guam and Hawaii. The *Columbia* landed on the dry lakebed at EAFB approximately 81.49 kilometers downrange of the reentry interface, which occurred at an altitude of 121 920 meters. Figures 4(a) to 4(j) contain some of the more pertinent trajectory data associated with the reentry of the Orbiter *Columbia*. All parameters are plotted as a function of flight Mach number and include time derivatives of the parameters required as inputs for sonic boom predictions using the method described in reference 1. These data were obtained using trajectory reconstruction techniques based on onboard instrumentation and ground-based radar and are considered to be the best estimate of the entry trajectory.

Pressure Measurement Instrumentation

The sonic boom data acquisition system used for the Space Shuttle STS-1 measurement program has been extensively performance proven by use in previous aircraft and Apollo 15 to 17 sonic boom measurement programs (refs. 9 to 12). This measurement system has been continually updated and currently uses a state-of-the-art time synchronization concept. A complete measurement system description is contained in reference 13. Eleven data acquisition stations (10 mobile and 1 fixed) were positioned along, under, and to the side of the STS-1 entry flightpath. (See fig. 3.) These systems consist of pressure transducers, dynagages (oscillator detector circuits), instrumentation amplifiers, frequency modulation (FM) magnetic tape recorders, and satellite time code receivers. The pressure transducer is a commercially available condenser microphone with a high frequency response to 10 kilohertz when used with the model DG-605 dynagage system; the low-end frequency response is approximately -5 decibels at 0.01 hertz. A photograph of a typical data acquisition system is shown in figure 5.

Figure 6 is a block diagram of a typical instrumentation system for sonic boom data acquisition. Typically, each measurement station recorded six channels of overpressure data, satellite time code reference, and voice annotation. These six overpressure ranges were derived from four microphones, three of which were co-located in a 1.2- by 1.2-meter (4 by 4 foot) ground board (necessary to obtain true ground pressures with the incident and reflected waves exactly in phase); the fourth microphone was mounted at a simulated-ear-level position. The output of the microphones was routed through appropriate signal-conditioning amplifiers which allowed various sensitivities for a range of overpressure levels. Laboratory calibration of this system to verify frequency response was performed at regular intervals. In the field, all tape recorder data channels were calibrated using a precision voltage source to verify center-frequency stability. The

microphones were calibrated using an acoustical calibrator which generated a known sound pressure level in a closed cavity at a fixed frequency of 1 kilohertz. These field calibrations were performed before and after reentry occurred to establish the amplitude sensitivity of the measurement system, which verified an end-to-end acoustical calibration.

Quantitative results from preoperational test (in the form of super-sonic flights using F-104 aircraft to generate the predicted overpressure ranges expected during this mission) verified that the sonic boom measurement system was operational. In figure 7, the instrumentation is shown as mounted in commercially available vehicles (vans) with electrical power being furnished by either portable gasoline generators or commercial power where applicable.

Atmospheric Soundings

Rawinsonde observations obtained at station 2 (Wheeler Ridge), which was positioned along the STS-1 reentry track 93 kilometers from the EAFB landing site, were taken at approximately 3 hours before and during STS-1 landing on April 14, 1981. Measured values of air temperature, wind direction, and windspeed as a function of altitude are given in table II for observations taken during the STS-1 landing. Rawinsonde data were obtained to an altitude of about 28 062 meters. Atmospheric data above 28 062 meters are based on a global reference atmosphere obtained from the National Weather Service.

RESULTS AND DISCUSSION

Signature Characteristics and Analysis

To ensure quality in the data acquisition, six overpressure measurements were actually recorded at each station location. The six overpressure signatures were obtained from four microphones, three of which were co-located at ground level with the fourth microphone mounted at a simulated-ear-level position as described earlier. This procedure has been used successfully in past sonic boom measurement programs (refs. 9 to 12). Each of the six measurements was then ranged differently (calibrated) in antici-pation of the possible variation of levels about the nominal or predicted level. In the following discussion, only the nominal ground level measurement (channel 1) and the ear level position measurement (channel 5) are used. All measurement stations were near the nominal or predicted level; consequently, these channels provide the most sensitive and better quality measurement.

The results presented herein were processed using the current state-of-the-art signal processing Fourier analyzer system; i.e., a Norland 3001 signal processing system and an HP5451C Fourier analyzer. These data were digitalized, calibrated (converted to engineering units in newtons per square meter), and then stored on floppy disk systems for subsequent retrieval, analysis, and plotting.

4

Figure 8 contains all the ground level signatures in an "iso-time history" format to compare the complete characteristics of the STS-1 entry signatures. Sonic boom signatures (instantaneous pressure time history) from all stations are presented in figures 9(a) to 9(k) for both ground level and ear level microphones. These results are plotted for a 0.8-second time period and are given in newtons per square meter for each of the 11 measurement stations. As discussed in the section entitled "Comparison With Predictions," the energy arriving at a given ground location originates at a specific point and altitude along the flightpath; i.e., Mach number. For stations which are located generally below the flightpath, the Mach number at which the energy originates decreases as the Orbiter approaches the landing site. With decreasing altitude and Mach number, a decrease in the duration of the sonic boom signatures is to be expected. This correlation is evident in figures 9(a) to 9(k) when comparing station 0 with station 10; i.e., Mach 5.87 with Mach 1.23. Also evident in these figures is the difference in arrival time between the incident and the reflected pressures at the ear level measurement (channel 5); this difference is discussed in more detail later. For example, figure 9(a) shows the incidence overpressure level at 17 N/m^2 followed later by the reflected wave at 34 N/m^2.

All flight signatures with the exception of that at $M = 5.87$ exhibited a shape very similar to theoretical N-waves. The $M = 5.87$ signature had a rounded peak, which is characteristic of signatures propagated from high altitudes and subjected to atmospheric turbulence (refs. 14 and 15). The peak positive and negative sonic boom levels and the duration for each location along with other typical sonic boom wave characteristics are summarized in table III.

Measurements were also inspected for any other type of signal events for a period of 2 minutes before and after the sonic boom arrival time of the signatures presented in figures 9(a) to 9(k). Measurements at station 4 (Camron Canyon) and station 9 (North Edwards) (figs. 10(a) and 10(b)) show a small reflected wave arriving shortly after the primary sonic boom wave; i.e., 0.210 second for station 4 and 0.120 second for station 9. Analyses indicate that these waves are due to reflections from nearby hills rather than to the direct propagation of energy from a different region along the flightpath.

Detailed analysis of the rise time of each signature at each measurement station has also been conducted. This analysis of the rise time is presented in figures 11(a) to 11(k) for an expanded 50-millisecond time interval for both the ground plane measurement and the ear level position measurements and is summarized in table III. The distinct difference in arrival time between the incident and the ground-reflected waves is clearly evident from the signatures recorded on the ear level measurements at all stations; i.e., the reflected wave is delayed in time from the incident wave. Because the ground plane and ear level measurements were located at slightly different positions with respect to the sonic boom wave front, the arrival times at these positions were slightly different, as can be seen. Consequently, the sonic boom arrival times shown in table III are determined using the ground plane measurement (channel 1).

The variation in delay time decreases with decreasing Mach number, as expected. This relationship is illustrated theoretically simply by

considering a wave front (wave normal) inclined at an angle θ with respect to the vertical. The delay time δ for a given height h above the ground can be expressed as

$$\delta = \frac{2h \, \cos \theta}{c}$$

where c is the atmospheric speed of sound.

If atmospheric refraction effects are ignored, for the moment, the angle θ can be related to Orbiter flight conditions as follows: $\theta = \phi - \psi$, where ϕ is the Mach angle ($\phi = \sin^{-1} (1/M)$) and ψ is the flightpath angle (measured positive downward from the horizontal in this simple illustration). As the Mach number M decreases, the Mach angle ϕ increases; consequently, the delay time can be expressed simply as

$$\delta = \frac{2h\sqrt{M^2 - 1}}{Mc}$$

The delay time of the reflected signature δ is summarized in table III, and this decrease with decreasing Mach number is evident.

Estimates of the ground reflection factor can be made with the aid of the ground plane and ear level measurements. Under simplifying assumptions of a plane wave front that is uniform over these two positions and because the incident wave (at the ear level position) is separated in time from the reflected wave, reasonable estimates are possible. For example, the ground plane measurement P_G inherently includes the reflection factor R_F; i.e., $P_G = R_F(P_I)$, where P_I is the incident pressure. The ear level measurement "incident pressure" P_E can be defined as $P_E = P_I$, $0 \leq t \leq \delta$, because the reflected pressure is delayed in time δ. Consequently, if the analysis is performed during the delayed time interval δ, then the ratio of P_G (ground plane) to P_E (ear level) should provide an approximation of the reflection factor; i.e., $P_G/P_E = (R_F P_I)/P_I = R_F$, $0 \leq t \leq \delta$. This operation was performed at each measurement station, and typical results are presented in figures 12(a) and 12(b) for stations 7 and 8, respectively. The ear level measurement had to be shifted in time before the ratio was performed, to account for the slightly different arrival time at the ground plane and ear level locations. The reflection factor estimates, summarized in table III, were obtained by averaging the reflection factor time signal over the latter position of the signals in figures 12(a) and 12(b).

The durations of the Orbiter entry sonic boom signatures are quite long in comparison to those of typical aircraft such as the SR-71 and the B-58 (ref. 14). They range from 375 milliseconds at $M = 1.23$ to 700 milliseconds at $M = 5.87$. Because of these long durations, the predominant energy of these signatures occurs at frequencies well below the normal hearing range of the human auditory system.

6

The dynamic response of any system is, of course, critically dependent not only on the dynamic characteristics of the system but also on the characteristics, both amplitude and frequency, of the input excitation. Consequently, to evaluate the effect of sonic booms on structures as well as people, the frequency content of the signature must be known.

When performing spectral analysis of transient signals, such as the sonic boom signature, energy spectral density (ESD) functions should be used instead of the power spectral density functions normally employed in analyzing stationary random signals (ref. 16). The ESD analysis is presented in figures 13(a) to 13(d) for the ground plane and ear level positions at two selected station locations. These results are typical of those at the other locations. In figures 13(a) and 13(b), the analysis is presented for a maximum frequency range of 2500 hertz. The rapid decay of energy with increasing frequency is clearly evident in these results. Also, the height effect of the ear level microphone elevation is clearly evident, by the introduction of additional lobing in the frequency spectrum. The analysis bandwidth resolution in these spectra is 1.22 hertz.

The results in figures 13(c) and 13(d) are presented to show, in more detail, the characteristics of the lower frequency portion of the spectra; i.e., below 100 hertz. The analysis bandwidth here is 0.244 hertz. The low frequency character of the STS-1 sonic boom signatures is clearly evident with the peak frequency slightly more than 2 hertz and the characteristic 6-dB/octave rolloff of these types of signals.

One additional comment concerning sonic boom measurements at elevation (ear level) should be made. The effect of elevation, as evident in the frequency spectrum in figure 13(b), is pronounced. The additional severe lobing, which is caused by the delay between the incident and the reflected pressures, occurs in the frequency range within the more sensitive region of the human auditory system. Slight changes in this delay δ, consequently, shift the lobing character in frequency. This shifting of the frequency character therefore could cause significant variation in the subjective evaluation of the sonic boom loudness even under seemingly identical conditions (ref. 17).

Comparison With Predictions

The technique described in reference 1 was used to extrapolate the near-field overpressure signature from flight conditions to the ground using the meteorological data shown in table II. The near-field signature data used are contained in references 7 and 8 as a function of Mach number, angle of attack, and ray angle. The Orbiter flight conditions from Mach 6 to Mach 1 which are also used in the predictions are shown in figure 4.

The process of identifying both the initial near-field signature and the trajectory state which correspond to the ground overpressure measurements recorded at the stations was iterative in nature. It consisted of a search on both the trajectory state and its companion near-field signature, which were systematically varied until the difference between the ground wave intersection point and the station locations of table I were matched.

Table IV is a summary of the results of this search and shows for each station the pertinent trajectory conditions, the signature ray angle, and the measured and predicted overpressures. A comparison between the positive portion of the predicted signatures defined by three points and the measured signatures is shown in figures 9(a) to 9(k) for all stations. In figure 14, the ground intersection of the overpressure at each Mach number is shown together with location of the measurement stations as a function of range from the runway threshold point. The predicted overpressure distribution as a function of lateral distance from the groundtrack for each Mach number is shown in figures 15(a) to 15(j) along with the measured levels.

CONCLUDING REMARKS

In this paper, sonic boom pressure signatures recorded during the entry of the Orbiter *Columbia* in the STS-1 mission are presented and compared with predictions. These signatures are similar to those generated from aircraft with the exception of longer durations and consequently lower peak frequency values. The peak overpressure levels recorded at 11 measurement stations ranged from 33.16 to 114.91 N/m^2. Peak levels and duration of the positive portion of the N-waves predicted using a semiempirical technique correlated well with the measured data. The mean differences between predicted and measured levels was 12 percent. Analysis of signature characteristics showed that the ground reflection factor varied from 1.83 to 2.32. A reflection factor of 1.9 was used for all predictions. The frequency analysis of the STS-1 signatures showed that the peak frequency of the Orbiter during entry is on the order of 2 hertz, which is much lower than that of typical military supersonic aircraft.

REFERENCES

1. Thomas, Charles L.: Extrapolation of Sonic Boom Pressure Signatures by the Waveform Parameter Method. NASA TN D-6832, 1972.

2. Hayes, Wallace D.; Haefeli, Rudolph C.; and Kulsrud, H. E.: Sonic Boom Propagation in a Stratified Atmosphere, With Computer Program. NASA CR-1299, 1969.

3. Hicks, Raymond M.; Mendoza, Joel P.; and Garcia, Frank, Jr.: A Wind Tunnel-Flight Correlation of Apollo 15 Sonic Boom. NASA TM X-62111, 1972.

4. Garcia, Frank, Jr.; Hicks, Raymond M.; and Mendoza, Joel P.: A Wind Tunnel-Flight Correlation of Apollo 16 Sonic Boom. NASA TM X-62073, 1973.

5. Holloway, Paul F.; Wilhold, Gilbert A.; Jones, Jess H.; Garcia, Frank, Jr.; and Hicks, Raymond M.: Shuttle Sonic Boom - Technology and Predictions. AIAA Paper 73-1039, Oct. 1973.

6. Malkin, Myron S.: Environmental Impact Statement for the Space Shuttle Program. Final Report. NASA TM-82278, 1978.

7. Mendoza, Joel P.: Wind Tunnel Pressure Signatures for a 0.0041-Scale Model of the Space Shuttle Orbiter. NASA TM X-62432, 1975.

8. Ashby, George C., Jr.: Near-Field Sonic-Boom Pressure Signatures for the Space Shuttle Launch and Orbiter Vehicles at Mach 6. NASA TP-1405, 1979.

9. Proceedings of the Sonic Boom Symposium. J. Acoust. Soc. America, vol. 39, no. 5, pt. 2, May 1966, pp. S1-S80.

10. Hilton, David A.; Henderson, Herbert R.; and McKinney, Royce: Sonic-Boom Ground-Pressure Measurements From Apollo 15. NASA TN D-6950, 1972.

11. Henderson, Herbert R.; and Hilton, David A.: Sonic-Boom Ground Pressure Measurements From the Launch and Reentry of Apollo 16. NASA TN D-7606, 1974.

12. Henderson, Herbert R.; and Hilton, David A.: Sonic-Boom Measurements in the Focus Region During the Ascent of Apollo 17. NASA TN D-7806, 1974.

13. Henderson, Herbert R.: Sonic Boom Measurement Test Plan for Space Shuttle STS-1 Reentry. NASA TM-85222, 1981.

14. Maglieri, Domenic J.: Sonic Boom Flight Research - Some Effects of Airplane Operations and the Atmosphere on Sonic Boom Signatures. Sonic Boom Research, A. R. Seebass, ed., NASA SP-147, 1967, pp. 25-48.

15. Maglieri, Domenic J.: Sonic Boom Ground Pressure Measurements for Flights at Altitudes in Excess of 70 000 Feet and at Mach Numbers up to 3.0. Second Conference on Sonic Boom Research, Ira R. Schwartz, ed., NASA SP-180, 1968, pp. 19-27.

16. Bendat, Julius S.; and Piersol, Allan G.: Engineering Applications of Correlation and Spectral Analysis. John Wiley and Sons (New York), 1980.

17. Johnson, D. R.; and Robinson, D. W.: Procedure for Calculating the Loudness of Sonic Bangs. Acustica, vol. 21, no. 6, 1969, pp. 307-318.

TABLE I.- STS-1 SONIC BOOM STATION LOCATIONS

Station	Lateral distance from groundtrack, km (a)	Station elevation, m	Station coordinates, deg:min:sec
0	-5.43	202	35:50:00 north 120:45:00 west
1	-6.00	116	35:09:38 north 119:20:29 west
2	-.87	148	35:04:50 north 118:57:29 west
3	4.82	1152	35:05:00 north 118:39:00 west
4	1.02	1402	35:04:10 north 118:19:30 west
5	-1.20	811	35:01:53 north 118:06:45 west
6	-1.02	750	35:00:21 north 118:00:45 west
7	.39	671	34:58:35 north 117:52:25 west
8	-12.11	695	34:51:38 north 117:52:32 west
9	9.96	693	35:02:39 north 117:47:24 west
10	-1.11	777	34:55:42 north 117:47:24 west

[a]Positive left of groundtrack.

10

TABLE II.- WHEELER RIDGE METEOROLOGICAL DATA

[1815 G.m.t., April 14, 1981]

Height, gpm[a]	Air temp., K	Wind dir, deg	Windspeed, m/sec	Height, gpm[a]	Air temp., K	Wind dir, deg	Windspeed, m/sec
168.0	295.7	330.0	0.5	4 727.8	265.5	186.9	4.6
194.0	294.5	286.7	.5	4 836.8	265.2	199.7	4.2
281.0	293.4	283.3	.7	4 960.9	264.3	206.6	4.5
368.5	292.3	280.9	.9	5 072.7	263.7	208.8	4.9
465.4	291.0	287.5	1.0	5 185.7	262.7	208.4	5.0
563.1	290.2	291.7	.7	5 314.3	261.4	205.2	4.8
652.6	289.4	257.8	.2	5 429.9	260.3	203.3	4.3
751.5	288.5	198.2	.6	5 546.8	259.2	204.1	4.0
842.9	288.1	169.6	.3	5 665.1	258.3	206.1	3.7
934.8	287.7	92.7	.2	5 784.8	257.5	204.4	3.4
1027.6	287.4	122.1	.2	5 905.9	256.0	194.7	3.3
1121.3	287.0	194.9	2.2	6 028.5	255.3	186.0	3.2
1215.9	286.6	167.4	3.4	6 152.8	254.6	184.4	2.6
1321.2	287.0	151.3	4.9	6 278.7	253.4	191.2	1.4
1418.5	289.0	132.8	7.2	6 406.1	252.1	183.7	1.4
1517.1	288.7	134.5	8.0	6 535.2	251.3	192.3	1.1
1606.7	287.9	134.9	8.3	6 649.6	250.1	220.8	.6
1707.0	287.0	133.4	7.8	6 781.9	248.7	255.8	.5
1808.2	286.2	131.3	7.3	6 899.0	247.3	290.3	.7
1910.3	285.4	129.0	7.8	7 034.4	246.0	303.6	1.1
2013.5	285.0	128.5	8.2	7 154.4	244.9	310.3	1.5
2117.7	283.5	127.7	8.4	7 275.9	243.7	301.9	1.2
2222.7	282.6	125.9	8.5	7 399.0	242.8	226.1	.9
2328.7	281.9	125.4	8.7	7 541.7	241.6	209.7	1.6
2425.0	280.6	126.5	8.7	7 668.4	240.8	223.7	2.3
2533.0	280.4	126.5	9.1	7 797.0	240.2	235.6	3.0
2642.1	279.0	127.3	9.3	7 927.6	239.2	242.1	3.5
2741.2	277.8	128.5	9.0	8 060.1	238.1	248.4	3.7
2852.2	277.0	132.4	8.4	8 175.1	236.7	256.8	3.7
2953.1	276.1	140.0	8.7	8 310.9	235.6	263.6	3.5
3055.1	276.1	146.9	9.6	8 448.8	234.3	267.8	3.1
3169.8	275.3	153.3	10.3	8 568.6	232.9	265.1	3.0
3274.1	274.5	160.6	9.9	8 710.3	232.1	258.5	3.3
3379.5	273.8	167.3	8.4	8 833.7	231.2	256.8	3.9
3486.1	273.7	166.6	7.4	8 979.9	229.9	263.4	4.6
3606.1	273.0	165.1	6.2	9 107.0	228.8	270.3	5.6
3703.0	271.9	162.5	5.1	9 236.2	228.2	266.9	6.6
3813.1	270.9	159.9	4.6	9 367.4	227.1	258.7	7.2
3924.3	270.0	156.0	4.3	9 523.2	226.2	254.0	7.7
4036.8	269.1	149.3	4.3	9 659.0	224.9	254.0	8.0
4150.5	268.3	147.4	4.7	9 796.9	223.9	257.0	8.1
4265.6	268.0	153.1	5.4	9 913.5	222.7	261.1	8.3
4382.2	267.6	161.5	6.0	10 055.7	222.1	268.4	8.8
4500.4	267.0	168.6	6.0	10 200.4	221.0	276.1	9.4
4606.8	266.4	176.9	5.3	10 347.8	219.9	284.3	9.7

[a]gpm = geopotential meters.

11

TABLE II.- Concluded

[1815 G.m.t., April 14, 1981]

Height, gpm[a]	Air temp., K	Wind dir, deg	Windspeed, m/sec	Height, gpm[a]	Air temp., K	Wind dir, deg	Windspeed, m/sec
10 472.7	219.1	288.5	9.7	18 428.3	215.0	247.1	4.6
10 625.2	218.0	288.6	9.4	18 606.6	217.0	212.6	4.3
10 754.5	217.4	287.6	9.3	18 885.0	216.9	206.4	7.2
10 912.9	216.7	290.2	9.3	19 176.0	216.7	206.6	9.3
11 047.3	215.7	291.1	9.6	19 377.4	216.4	209.8	9.7
11 212.0	215.2	285.0	9.9	19 691.1	215.4	207.9	6.3
11 352.2	214.3	273.5	11.1	19 909.1	216.2	213.7	6.5
11 524.0	213.8	268.3	12.5	20 251.7	216.4	233.3	4.8
11 670.7	213.6	271.6	13.2	20 490.9	216.2	248.3	2.1
11 820.7	213.3	278.9	12.9	20 866.9	215.7	180.2	2.7
11 943.2	213.3	282.9	11.1	21 131.2	217.4	96.2	3.1
12 099.5	212.4	275.0	9.6	21 408.0	217.0	147.6	1.1
12 259.5	212.2	260.3	9.9	21 847.0	217.4	269.9	.8
12 423.8	212.8	251.3	11.4	22 318.0	216.5	101.9	7.1
12 558.8	213.6	248.0	12.0	22 653.4	218.3	79.1	9.9
12 732.2	213.6	246.8	11.9	23 195.1	219.0	27.9	6.4
12 874.4	213.5	245.7	11.9	23 584.4	219.4	52.6	8.3
13 057.0	214.0	243.4	12.5	24 002.1	222.4	44.8	8.6
13 207.7	215.4	241.2	12.6	24 692.1	224.6	51.4	9.8
13 362.5	215.4	239.7	12.4	25 199.0	225.1	55.3	13.0
13 521.7	216.4	239.6	12.6	26 043.6	225.9	41.2	10.0
13 685.0	215.7	240.9	12.9	26 669.9	222.7	30.2	8.9
13 852.4	215.5	241.6	12.7	27 741.4	227.4	353.1	8.5
14 024.3	215.7	238.5	12.8	29 045.9	231.3	331.8	10.4
14 200.9	215.4	233.9	13.5	30 500.0	232.8	120.6	.5
14 382.5	215.4	229.3	14.7	32 300.0	237.0	296.6	.5
14 569.3	214.9	228.6	15.5	34 100.0	241.1	298.3	1.5
14 761.5	214.9	230.3	15.6	36 000.0	245.4	297.1	2.3
14 909.3	213.8	233.5	15.1	37 800.0	249.7	295.5	2.9
15 111.9	214.9	234.5	13.6	39 600.0	254.0	294.5	3.5
15 268.9	215.7	229.7	13.9	41 500.0	258.8	270.9	3.7
15 485.0	215.7	227.5	16.5	43 300.0	263.7	247.1	4.5
15 652.3	216.4	228.9	16.5	45 100.0	268.1	233.6	5.8
15 824.7	217.0	232.4	15.6	46 900.0	269.3	243.4	6.2
16 062.0	216.4	234.0	14.7	48 800.0	270.5	251.8	6.7
16 245.8	216.4	231.5	12.4	50 600.0	270.5	254.3	6.7
16 434.8	215.7	223.8	11.3	52 400.0	267.7	244.8	5.4
16 628.9	215.0	218.4	12.0	54 300.0	265.1	230.3	4.4
16 828.1	213.3	220.4	13.8	56 100.0	261.1	208.4	4.1
17 032.5	212.2	225.0	16.2	57 900.0	256.1	186.1	4.5
17 243.3	212.2	230.4	15.7	59 700.0	251.0	169.8	5.5
17 461.9	212.9	237.3	12.6	61 600.0	246.2	165.0	4.1
17 689.2	213.6	237.3	12.1	63 400.0	241.3	156.7	2.4
17 925.2	213.3	241.8	11.3	65 200.0	236.4	135.9	.9
18 171.2	216.9	253.9	8.3				

[a]gpm = geopotential meters.

TABLE III.- STS-1 SONIC BOOM MEASURED OVERPRESSURE CHARACTERISTICS

Measurement location		Peak overpressure level, N/m²		Total time duration, sec	Rise time, msec	Boom arrival time G.m.t., hr:min:sec	Reflected signature delay δ, msec	Reflection factor
Station no.	Channel no.	Positive	Negative					
0	1	33.16	27.39	0.693	4.4	18:13:28.432	8.6	1.84
	5	34.33	31.85	.700	4.2			
1	1	58.41	54.58	0.583	5.0	18:14:47.579	8.6	1.87
	5	61.77	57.9	.588	5.0			
2	1	44.53	41.18	0.530	4.0	18:15:08.729	9.0	2.27 to 2.32
	5	38.30	38.3	.538	4.0			
3	1	54.58	53.98	0.525	4.4	18:15:29.283	8.2	2.09
	5	50.75	56.98	.531	4.2			
4	1	76.61	73.74	0.491	4.8	18:15:54.266	8.6	2.00
	5	68.47	67.03	≈.497	4.6			
5	1	75.17	72.78	0.402	≈4.4	18:16:20.651	8.0	1.98
	5	75.17	74.21	≈.414	≈4.4			
6	1	114.91	105.82	0.394	4.0	18:16:33.797	8.0	--
	ᵃ5	86.18	90.01	.406	--			
7	1	93.85	84.75	0.380	≈4.0	18:16:54.366	7.2	1.85
	5	101.03	90.97	.393	--			
8	1	86.66	79.00	0.376	5.0	18:17:11.449	5.4	1.98
	5	81.40	Clipped	Clipped	5.0			
9	1	108.21	90.49	0.375	3.6	18:17:08.634	5.4	1.90
	5	94.32	89.54	.380	2.8			
10	1	89.04	83.31	0.375	1.8 to 3.2	18:17:17.103	5.8	1.83
	5	79.48	105.82	.380	≈1.8			

ᵃChannel very noisy.
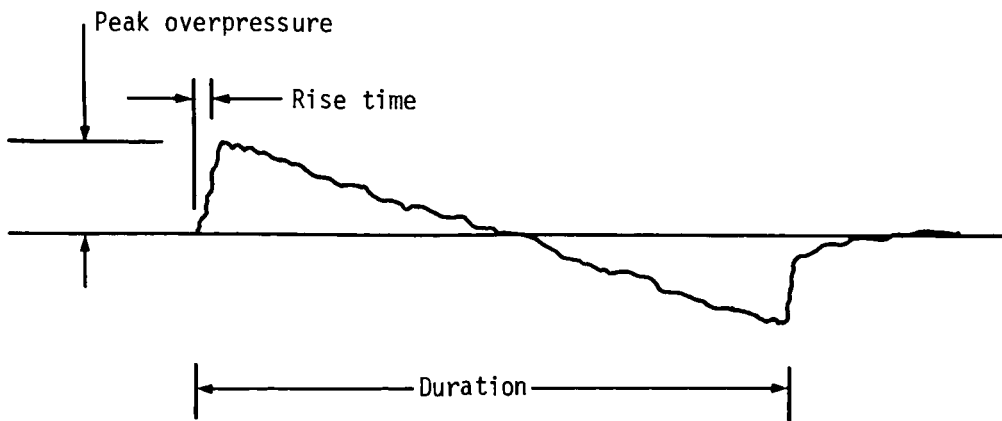
Classic N-wave characteristics

13

TABLE IV.- COMPARISON OF PREDICTED AND MEASURED PEAK OVERPRESSURE LEVELS

Station	Boom origin time G.m.t., hr:min:sec	Mach number	Altitude, m	Ray angle,[a] deg	Ray travel time, sec	Predicted ΔP, N/m^2	Recorded ΔP, N/m^2
0	18:11:19	5.87	39 337	-8.5	129.7	35.91	33.16
1	18:12:56	3.94	32 876	-11	111.5	48.26	58.41
2	18:13:27	3.41	30 401	-2	101.3	55.88	44.53
3	18:13:56	2.97	27 899	+10	92.1	54.44	54.58
4	18:14:32	2.39	24 953	+2	82.6	71.58	76.61
5	18:15:01	1.98	23 054	-4	79.4	87.48	78.04
6	18:15:18	1.76	21 552	-4	75.1	92.65	114.91
7	18:15:41	1.45	19 447	0	73.0	92.98	93.85
8	18:15:41	1.45	19 447	-36	90.6	75.17	86.66
9	18:15:45	1.40	19 103	+30	83.9	80.63	108.21
10	18:16:01	1.23	17 770	-6	76.5	87.43	89.04

[a]Angle at which ray leaves Orbiter, positive left of groundtrack.

Definition of the ray angle
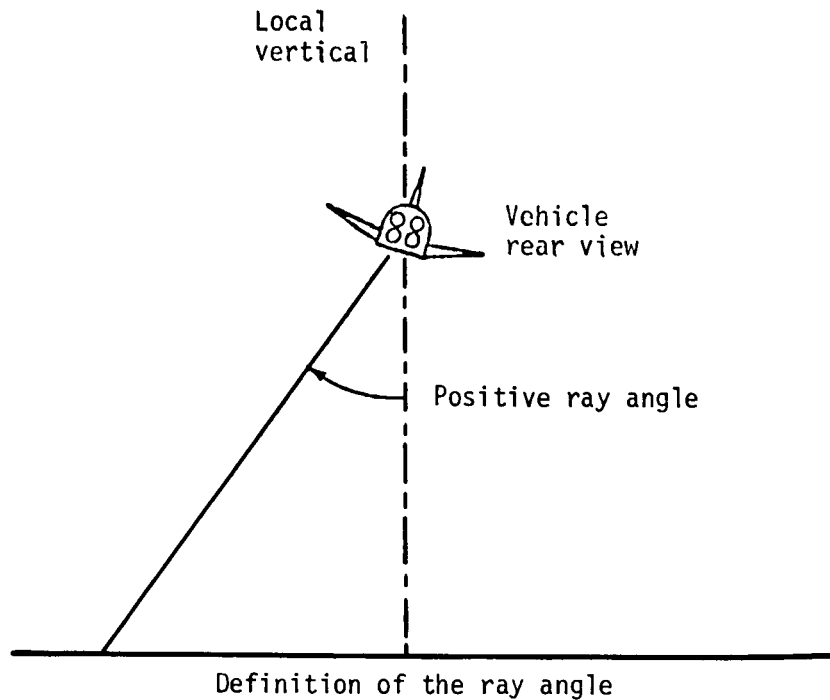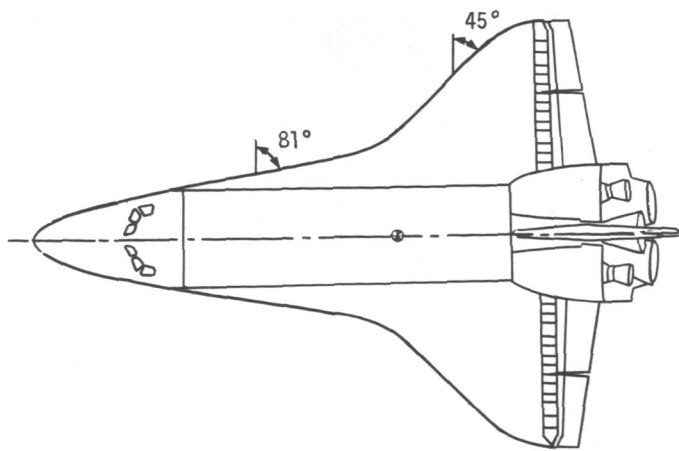
Reference dimensions

Area	$S = 250$ m^2
Mean aerodynamic chord	$\bar{c} = 12.06$ m
Center of gravity	$x = 21.30$ m
Length	$l = 32.77$ m
Span	$b = 23.79$ m

45°

81°

Center of gravity = 0.65l

10.56 m

32.77 m

23.79 m
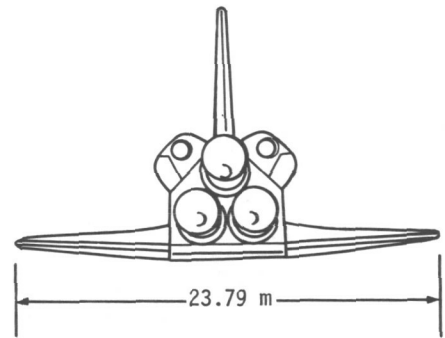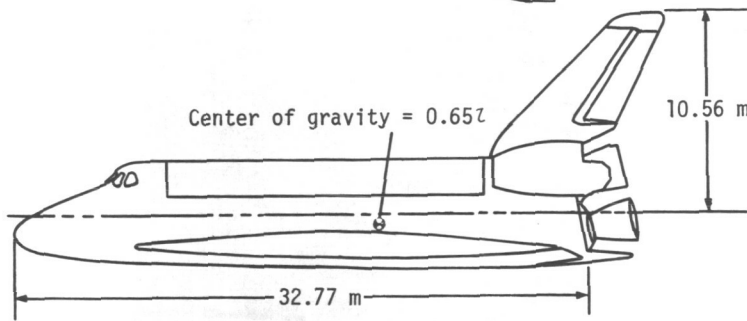
Figure 1.- Schematic of Orbiter configuration.
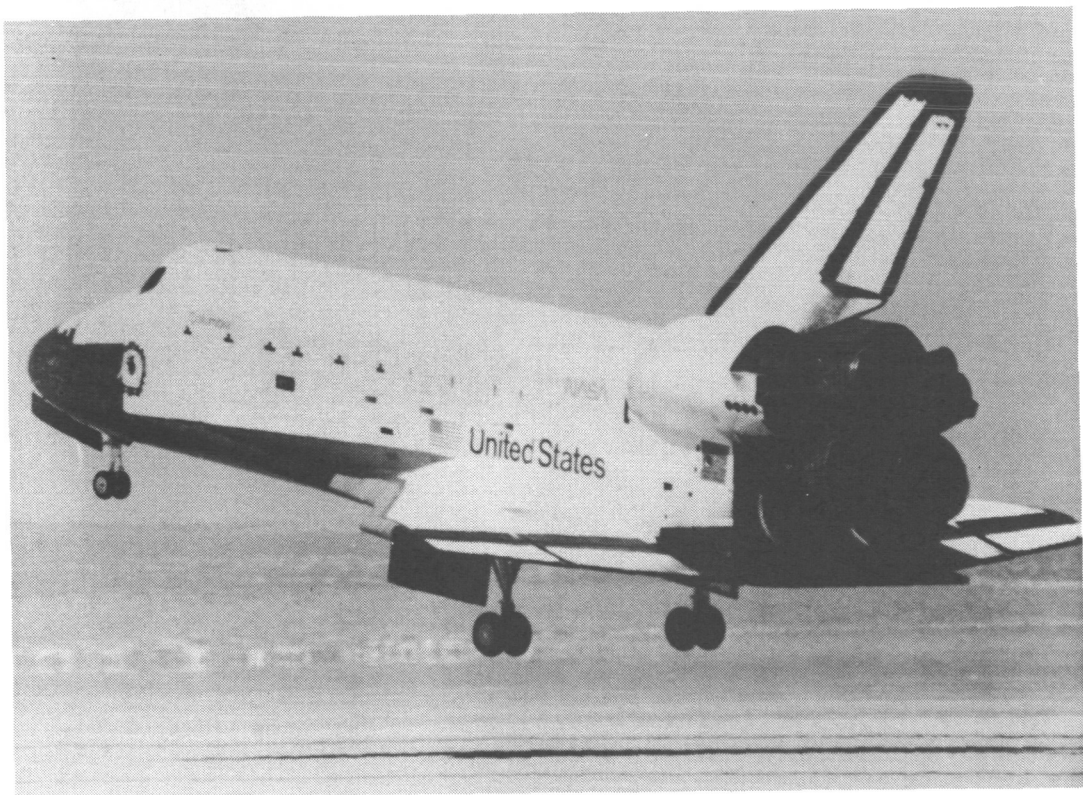
Figure 2.- Orbiter *Columbia* nearing touchdown.
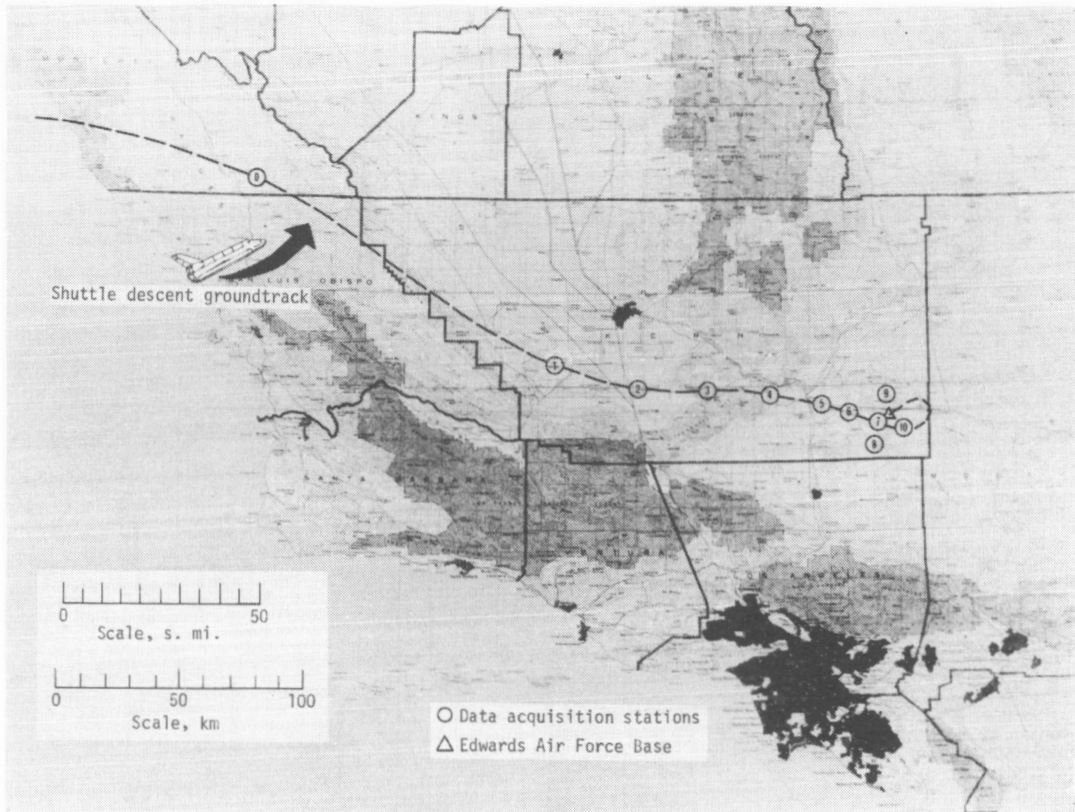
Figure 3.- Reentry groundtrack and measurement stations.
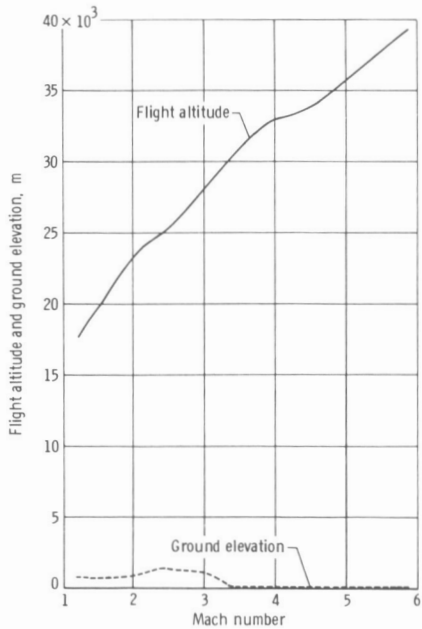
(a) Altitude and ground elevation.

Figure 4.- Best estimated trajectory
data history for sonic boom
predictions.
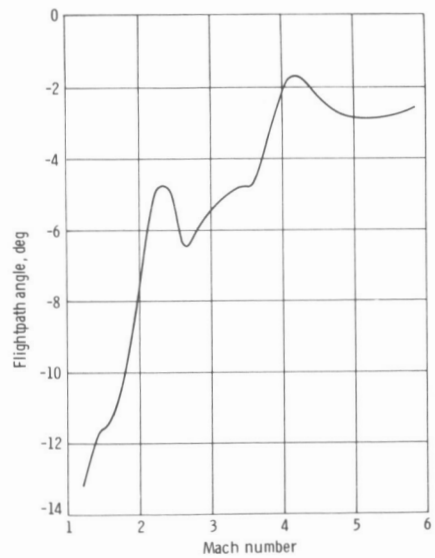
(b) Flightpath angle.

Figure 4.- Continued.

16
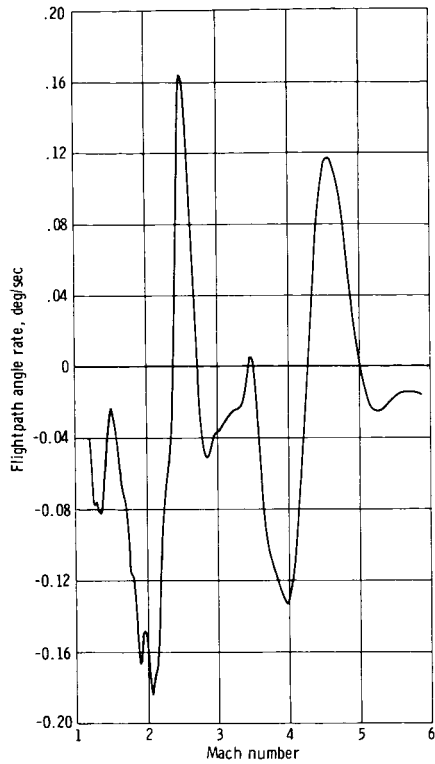
(c) Flightpath angle rate.
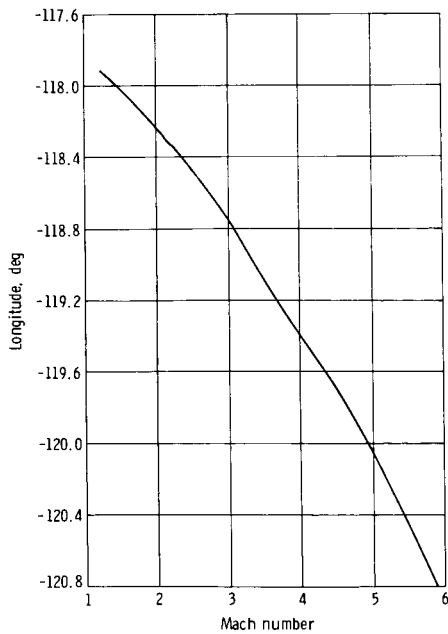
Figure 4.- Continued.

(d) Mach rate.

Figure 4.- Continued.

(e) Longitude.
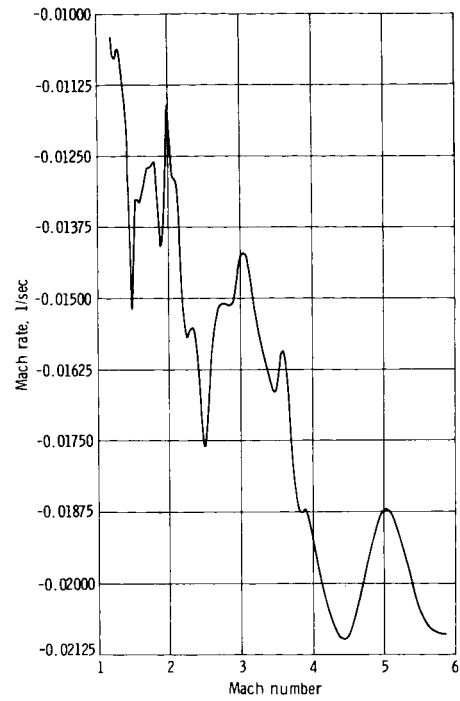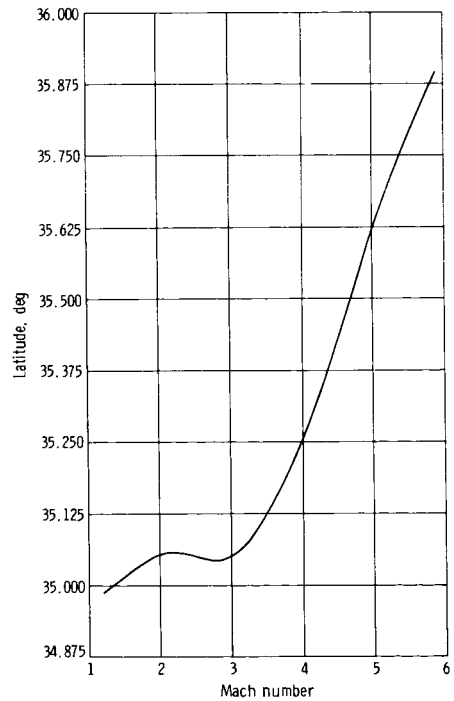
Figure 4.- Continued.

(f) Latitude.

Figure 4.- Continued.

17
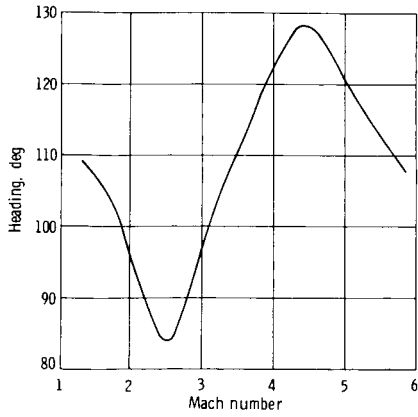
(g) Heading.

Figure 4.- Continued.
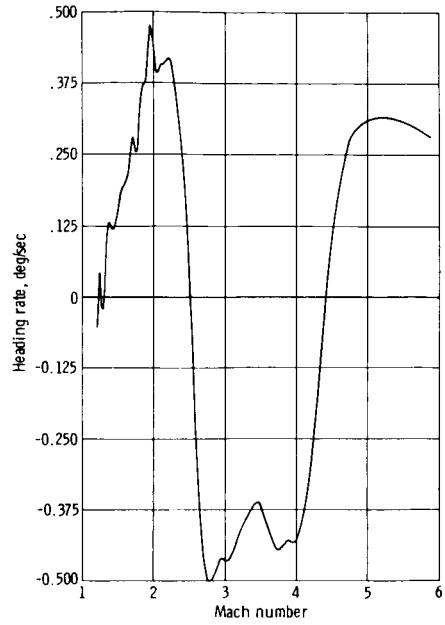
(h) Heading rate.

Figure 4.- Continued.
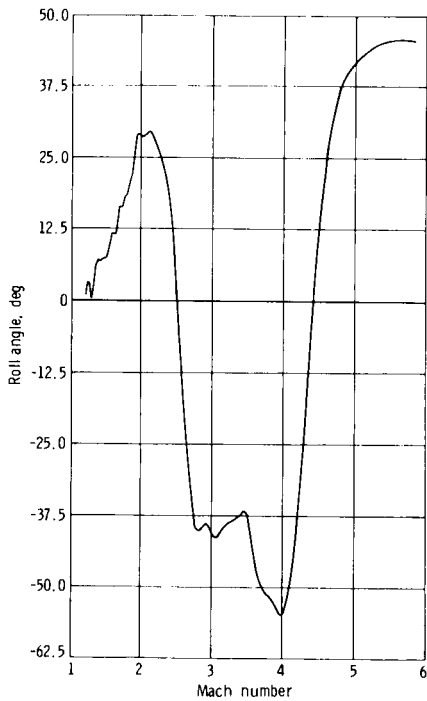
(i) Roll angle.

Figure 4.- Continued.
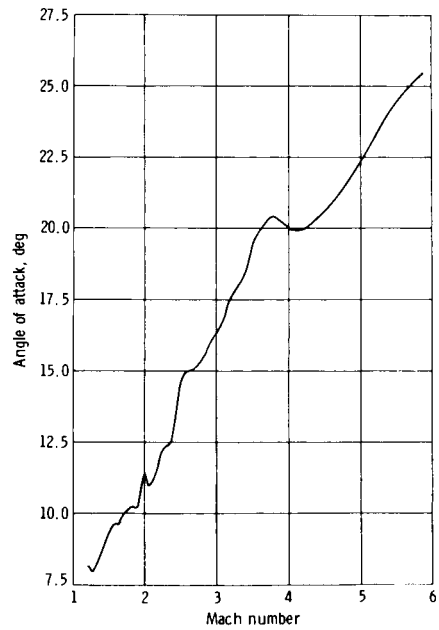
(j) Angle of attack.

Figure 4.- Concluded.

18

Figure 5.- Typical sonic boom data recording equipment.

1 - PHOTOCON CONDENSER MICROPHONE MODEL 464
2 - PHOTOCON CABLE TERMINATION NETWORK (100') MODEL 257 3N
3 - PHOTOCON DYNAGAGE TUNER MODEL DG-605
4 - PHOTOCON POWER SUPPLY MODEL PS-605
5 - BURR-BROWN MULTI CHANNEL POWER SUPPLY MODEL 506/16A
6 - BURR-BROWN AMPLIFIER MODEL 3640-1
7 - SATELLITE TIME CODE RECEIVER TRUE TIME MODEL 468-DC
8 - F. M. TAPE RECORDER TYPICAL MODEL HONEYWELL 5600
9 - SIGNAL MONITOR PANEL
10 - WINCO PORTABLE GASOLINE GENERATOR MODEL 305BH-1MJ

Figure 6.- Data acquisition system schematic.
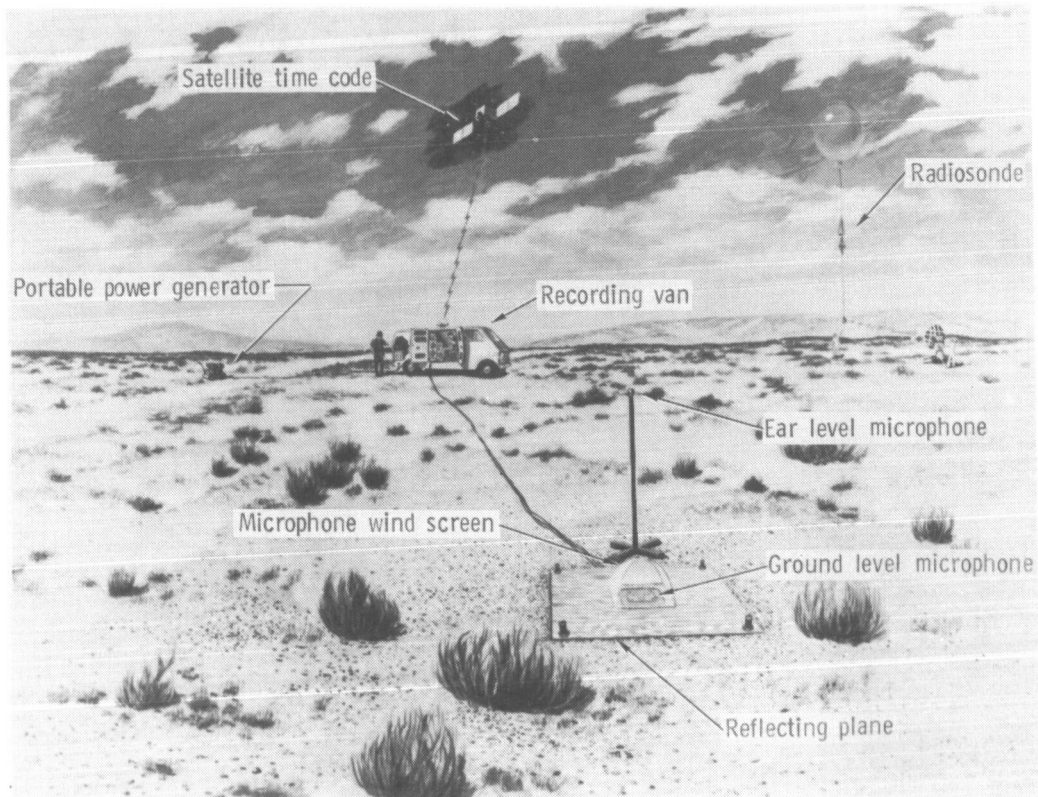
Figure 7.- Field layout of data acquisition system.

Overpressure

$\triangle P$, N/m^2

Conditions at which booms were generated

0.1 sec

Station	$\triangle P$		Altitude, m
0	33.16	M = 5.87	39 337
1	58.41	M = 3.94	32 876
2	44.53	M = 3.41	30 401
3	54.58	M = 2.97	27 899
4	76.61	M = 2.39	24 953
5	78.04	M = 1.98	23 054
6	114.91	M = 1.76	21 552
7	93.85	M = 1.45	19 447
8	86.66	M = 1.45	19 447
9	108.21	M = 1.40	19 103
10	89.04	M = 1.23	17 770
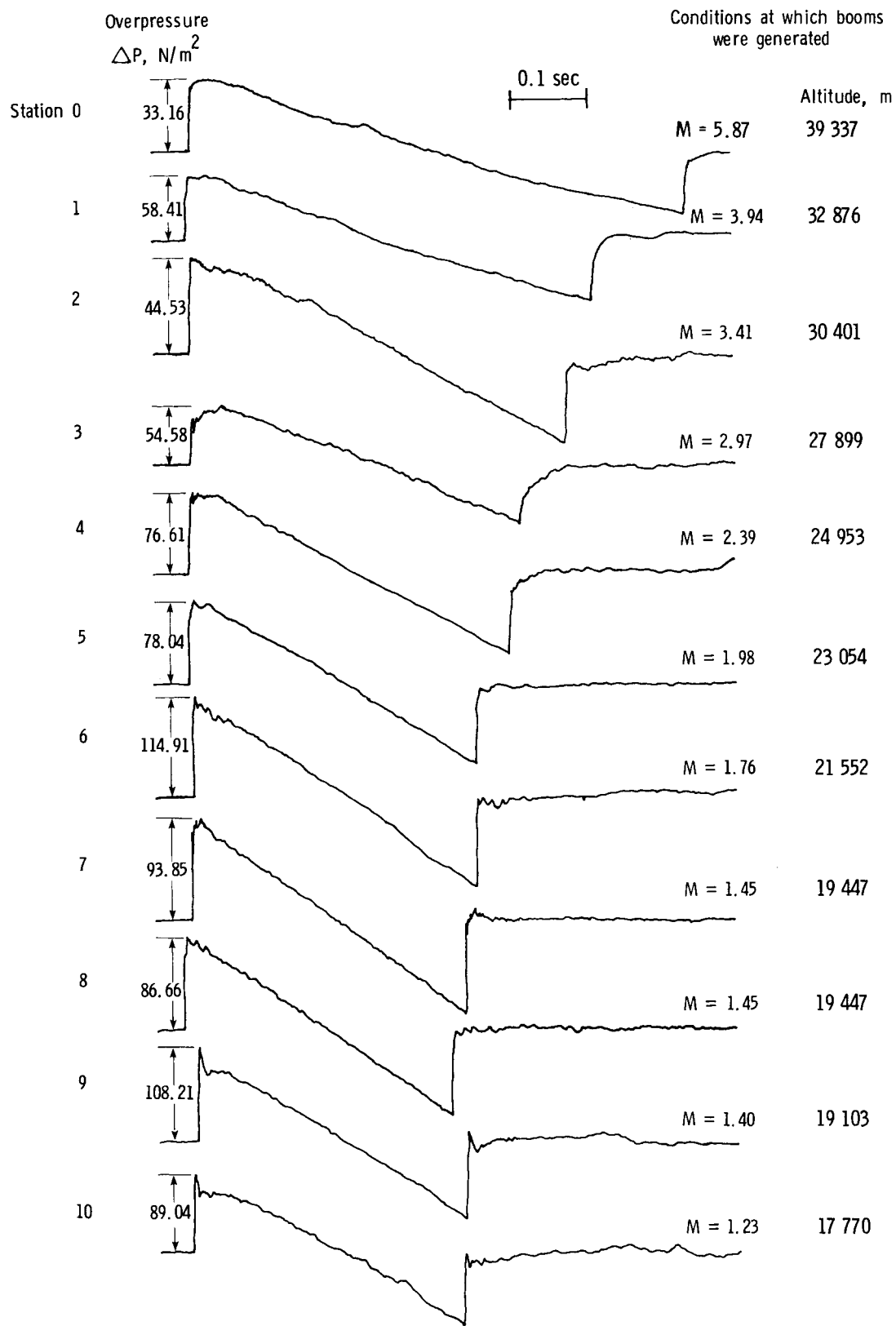
Figure 8.- Measured sonic boom signatures recorded at 11 measurement sites located under and lateral to the STS-1 reentry groundtrack.

21
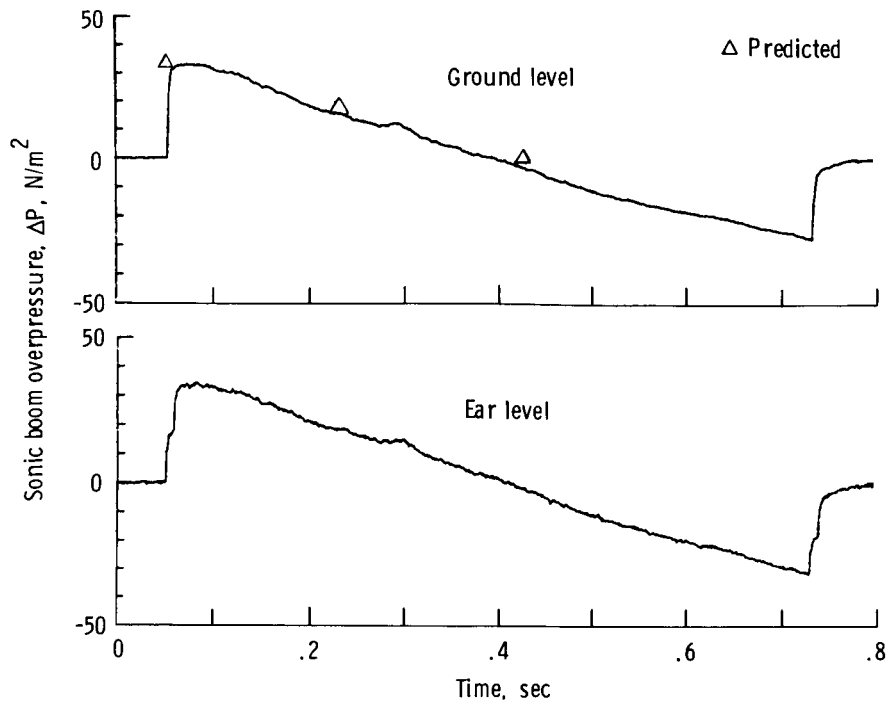
(a) Station 0.

Figure 9.- Predicted and measured sonic boom signatures.
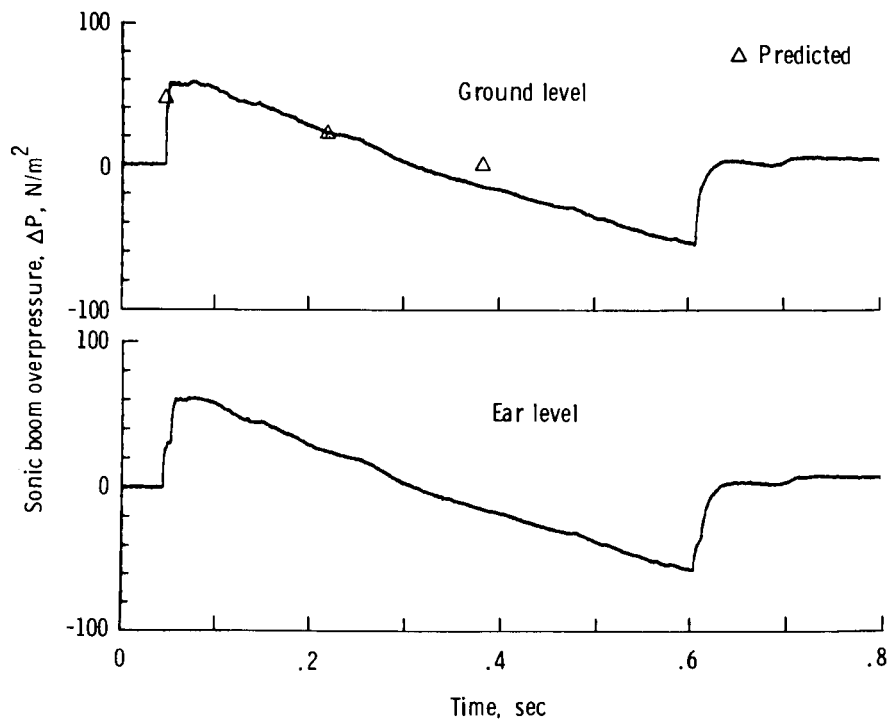
(b) Station 1.

Figure 9.- Continued.
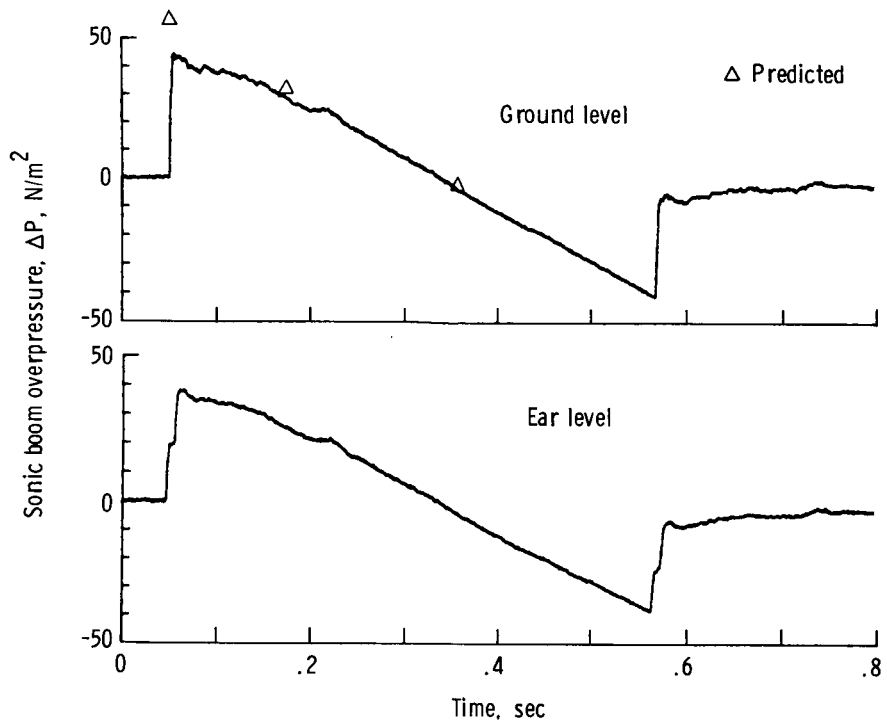
(c) Station 2.

Figure 9.- Continued.
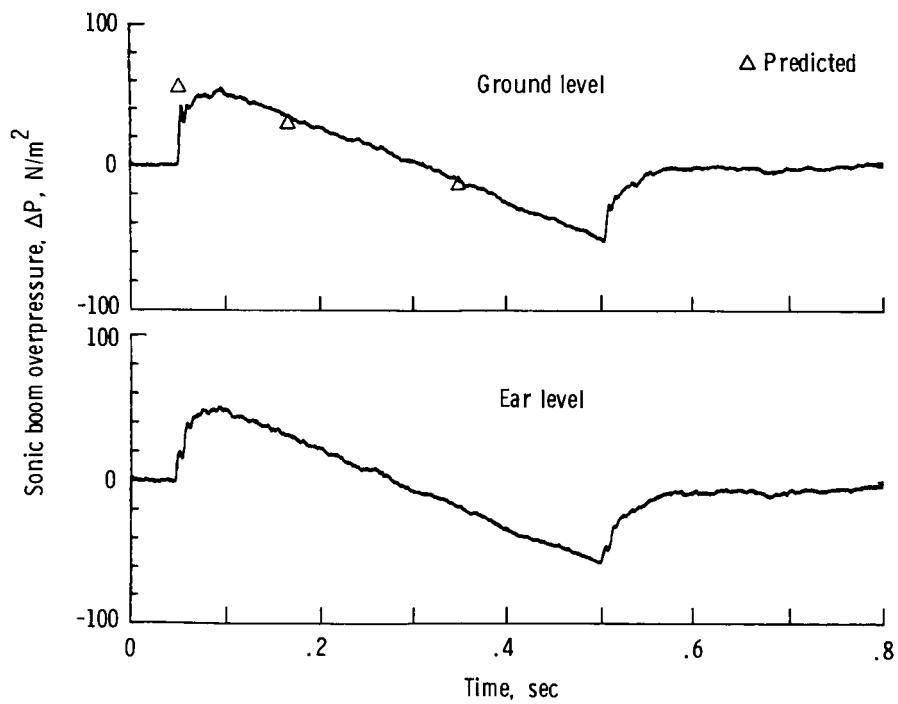
(d) Station 3.

Figure 9.- Continued.
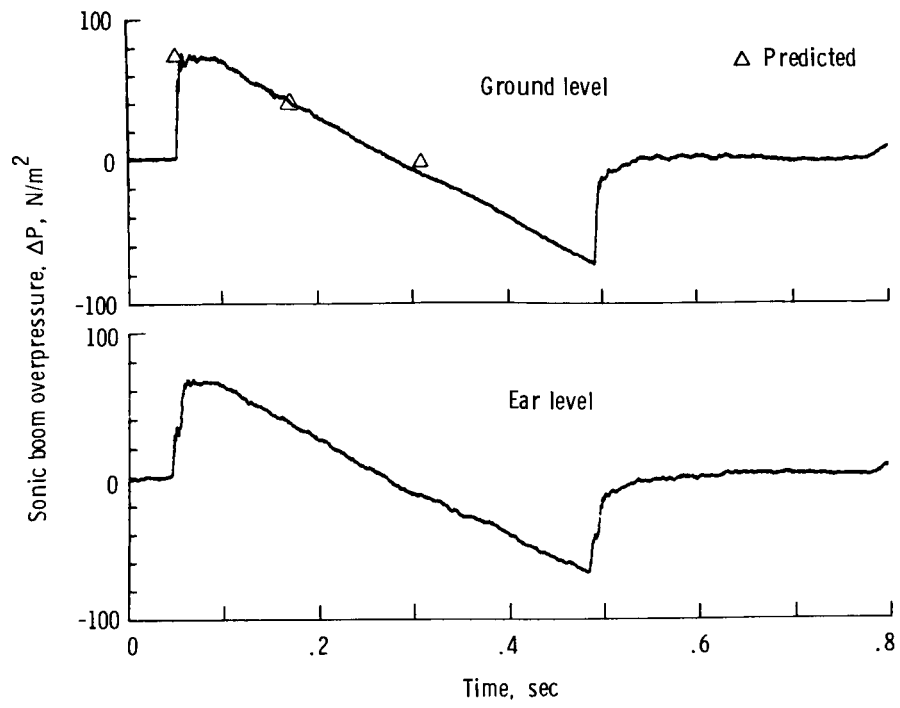
(e) Station 4.

Figure 9.- Continued.
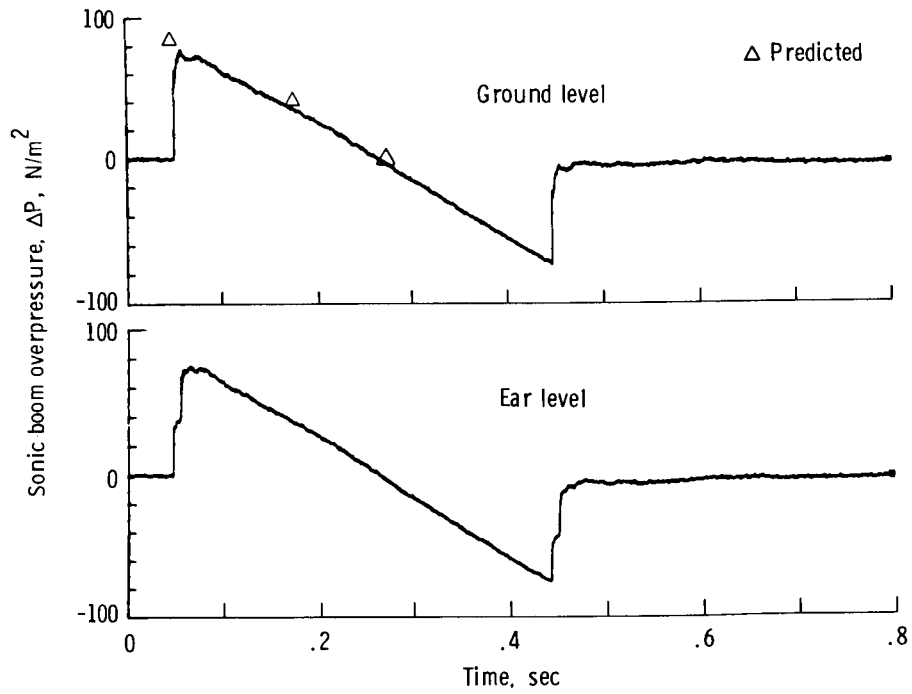
(f) Station 5.

Figure 9.- Continued.
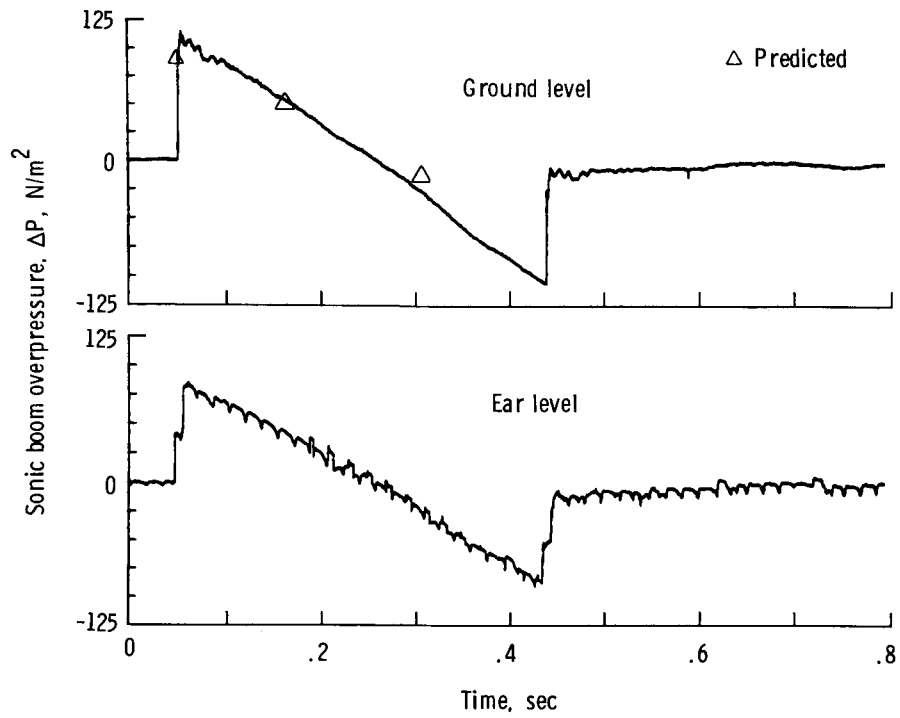
(g) Station 6.

Figure 9.- Continued.
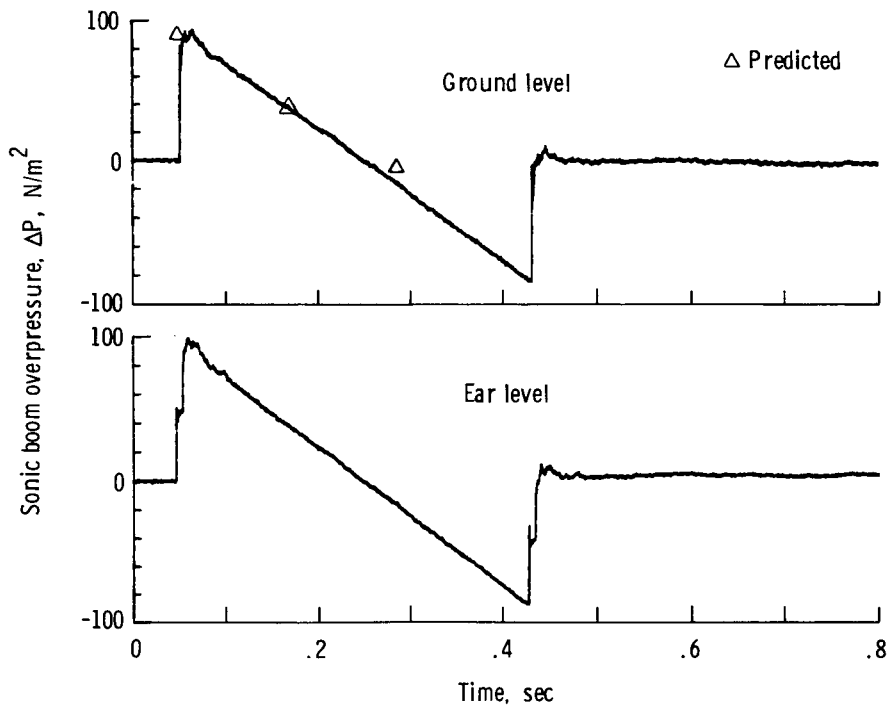
(h) Station 7.

Figure 9.- Continued.
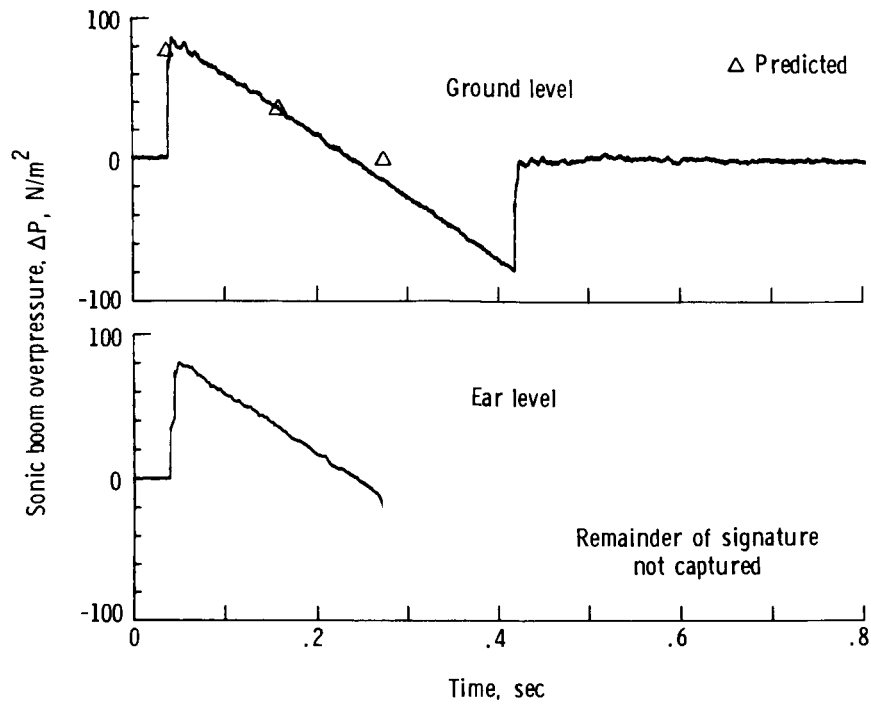
(i) Station 8.

Figure 9.- Continued.
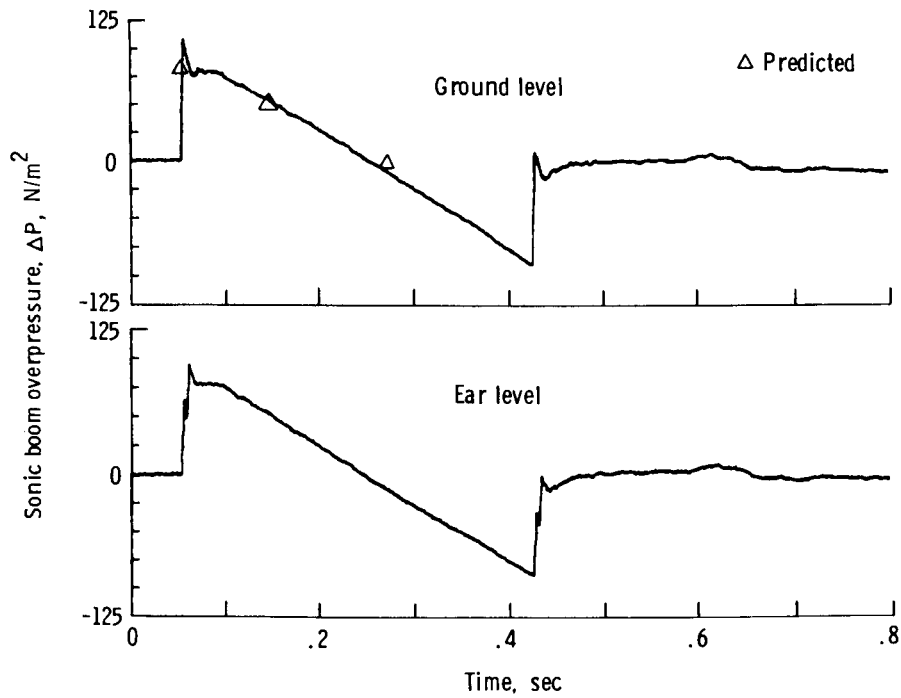
(j) Station 9.

Figure 9.- Continued.
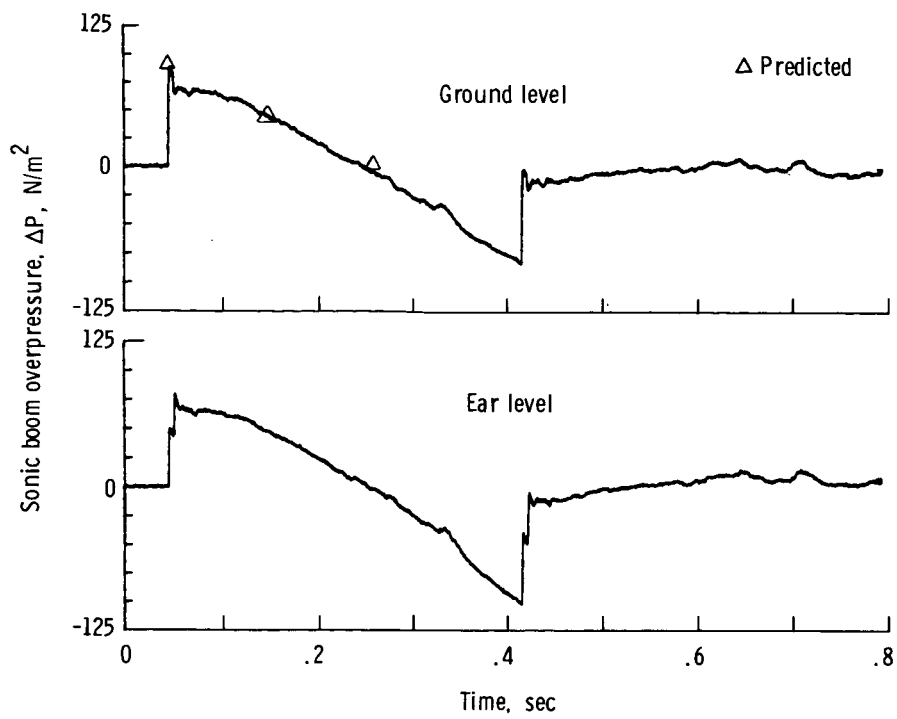
(k) Station 10.

Figure 9.- Concluded.
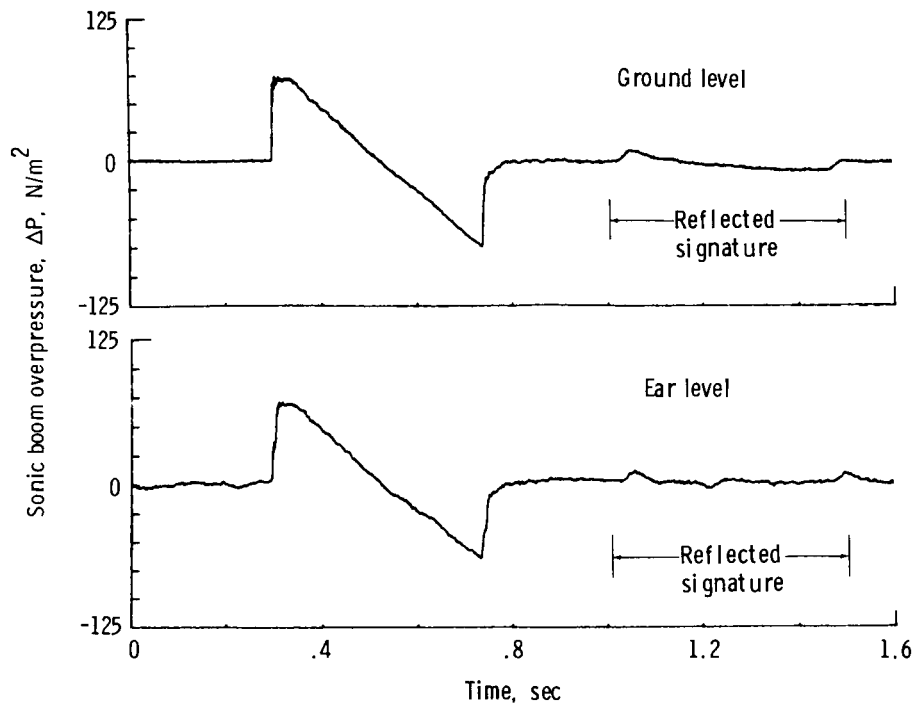
(a) Station 4.

Figure 10.- Direct and reflected sonic boom signatures.
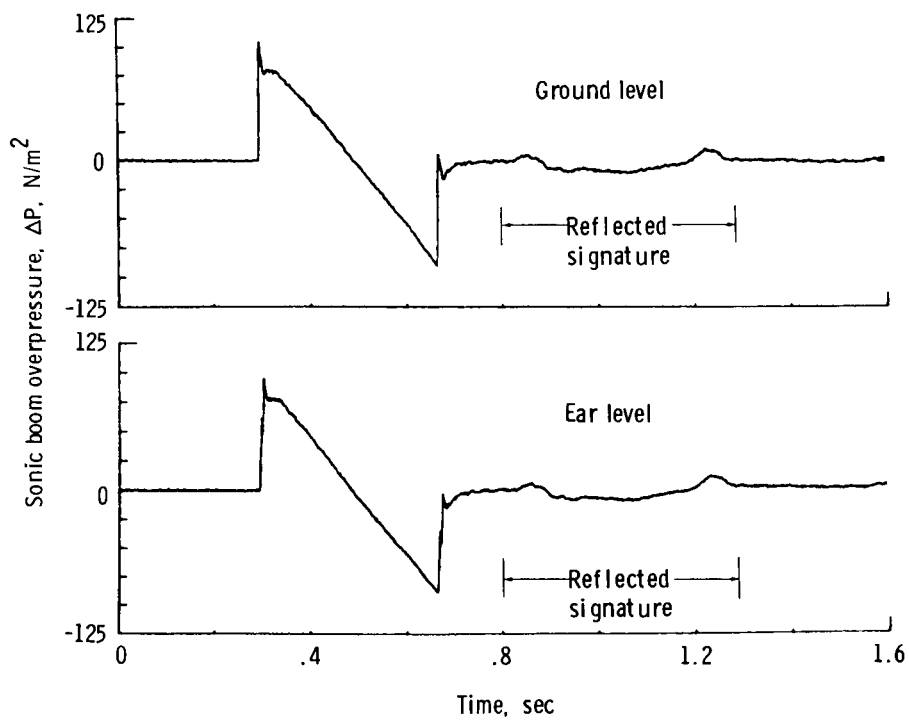
(b) Station 9.

Figure 10.- Concluded.
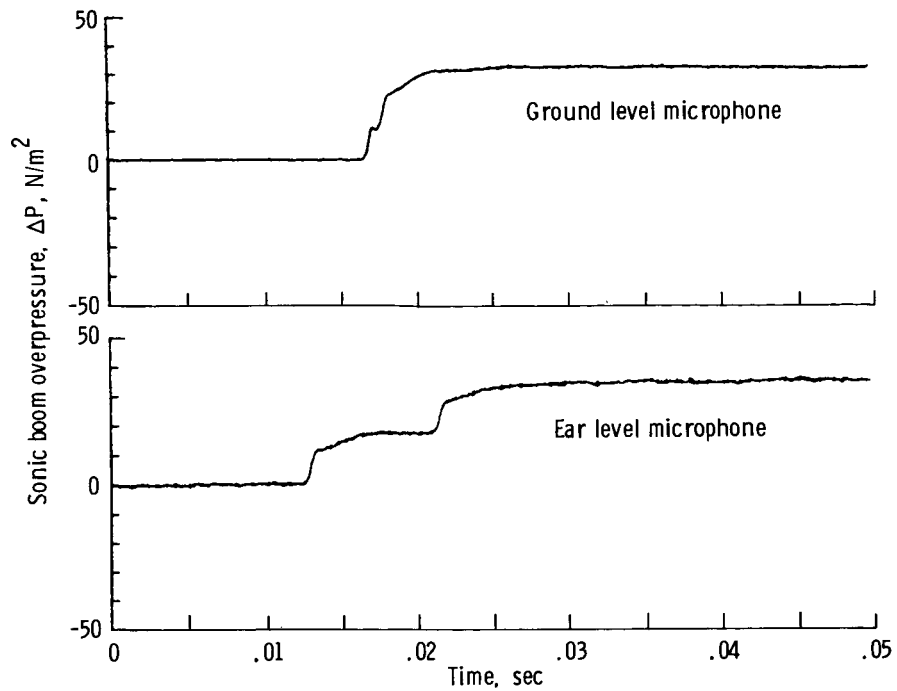
(a) Station 0.

Figure 11.- Pressure rise time of sonic boom.
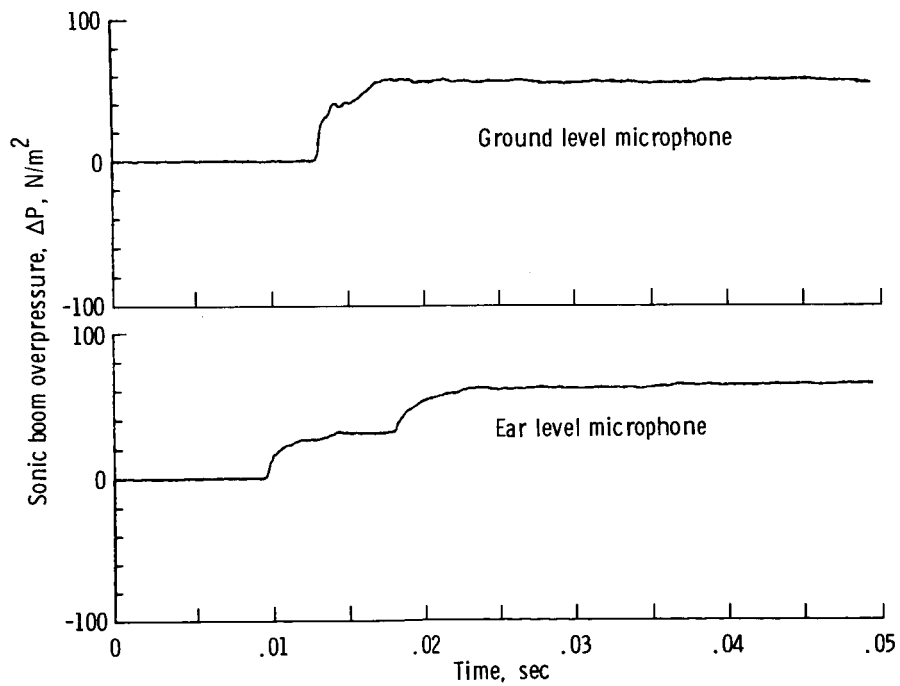
(b) Station 1.

Figure 11.- Continued.

29
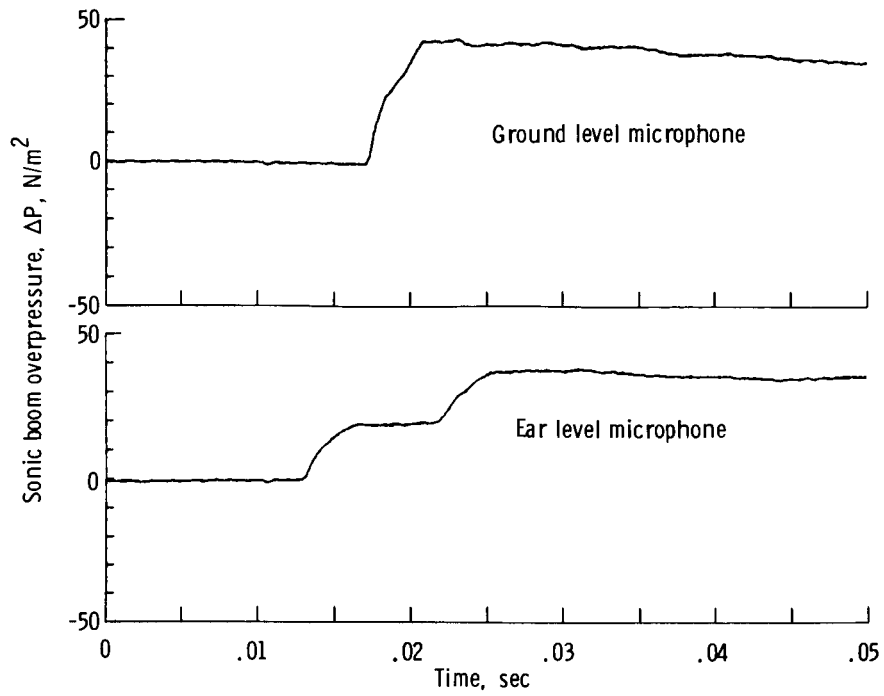
(c) Station 2.

Figure 11.- Continued.
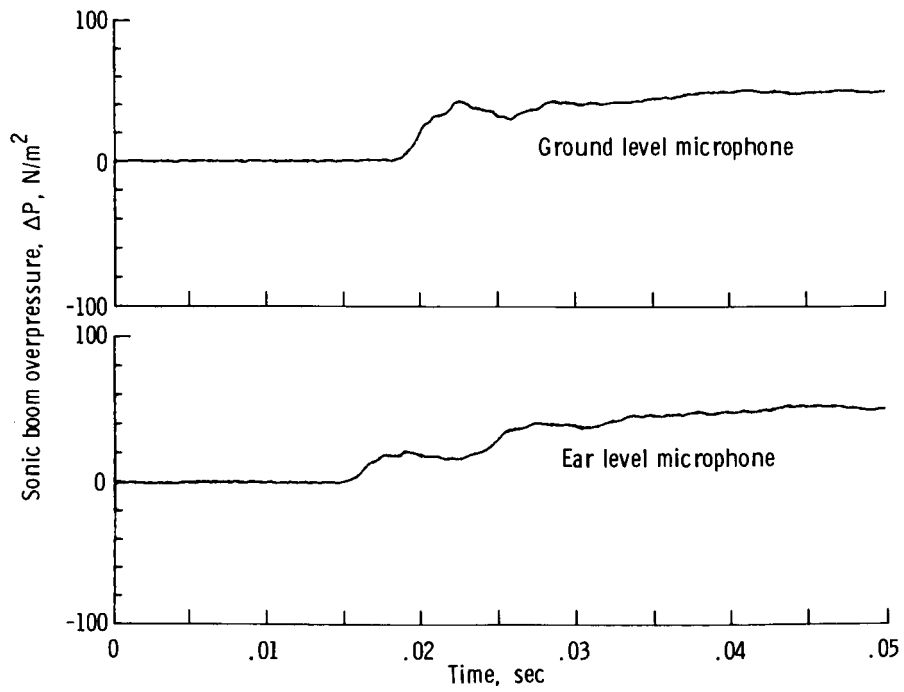
(d) Station 3.

Figure 11.- Continued.
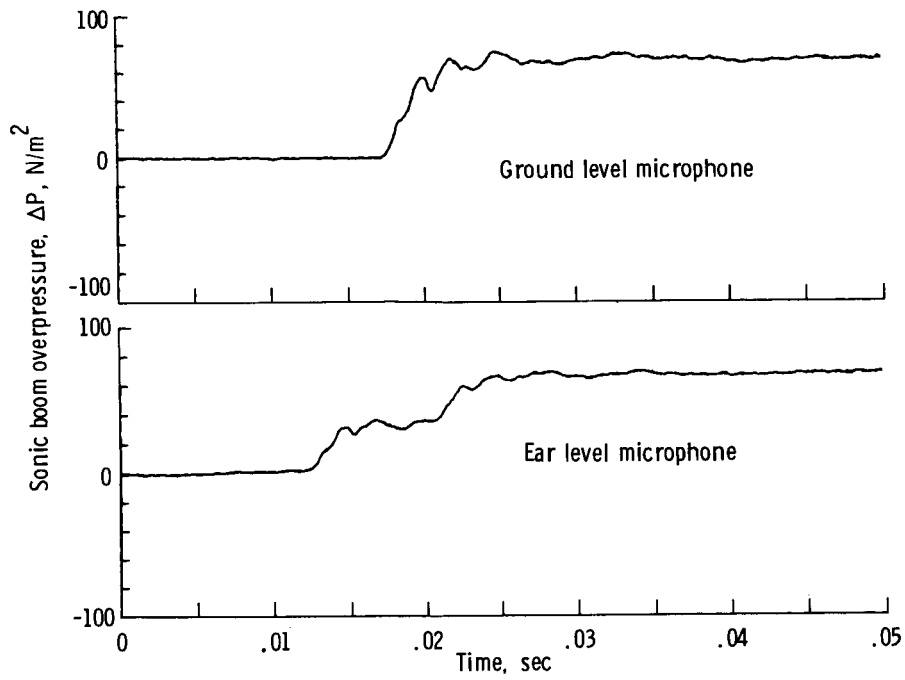
(e)   Station 4.

Figure 11.- Continued.
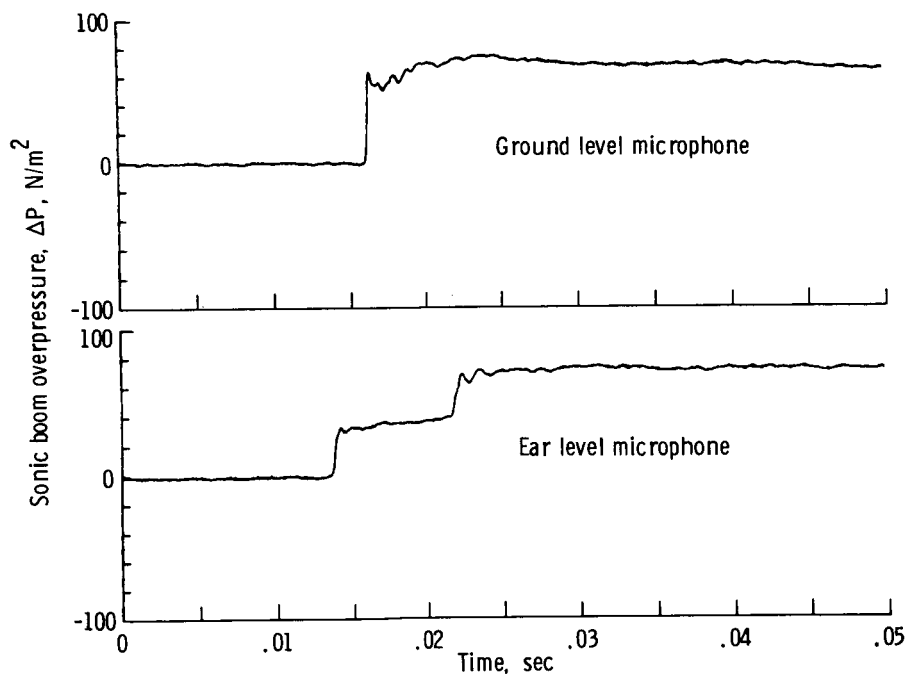
(f)   Station 5.

Figure 11.- Continued.
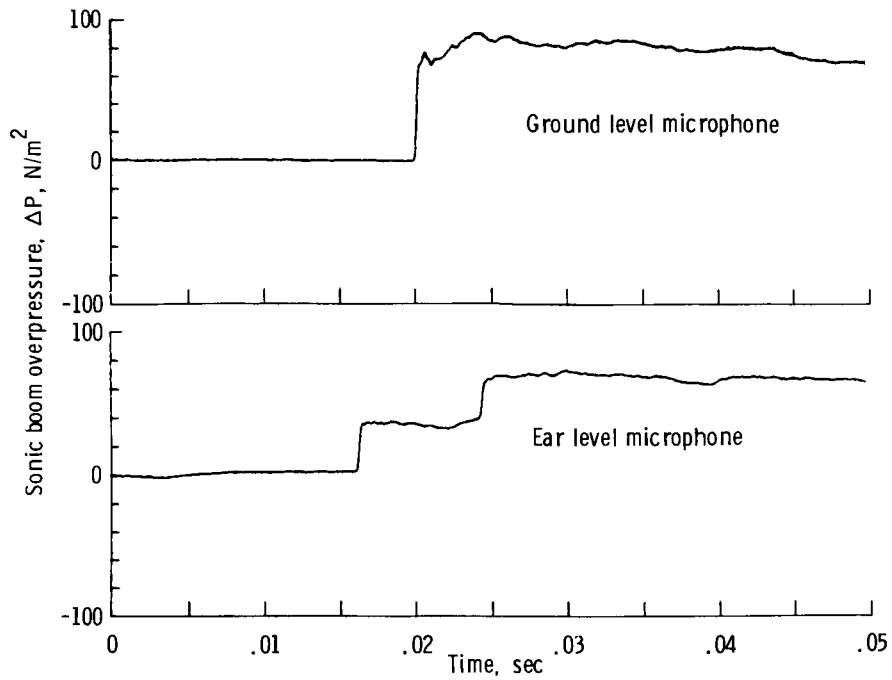
(g) Station 6.

Figure 11.- Continued.
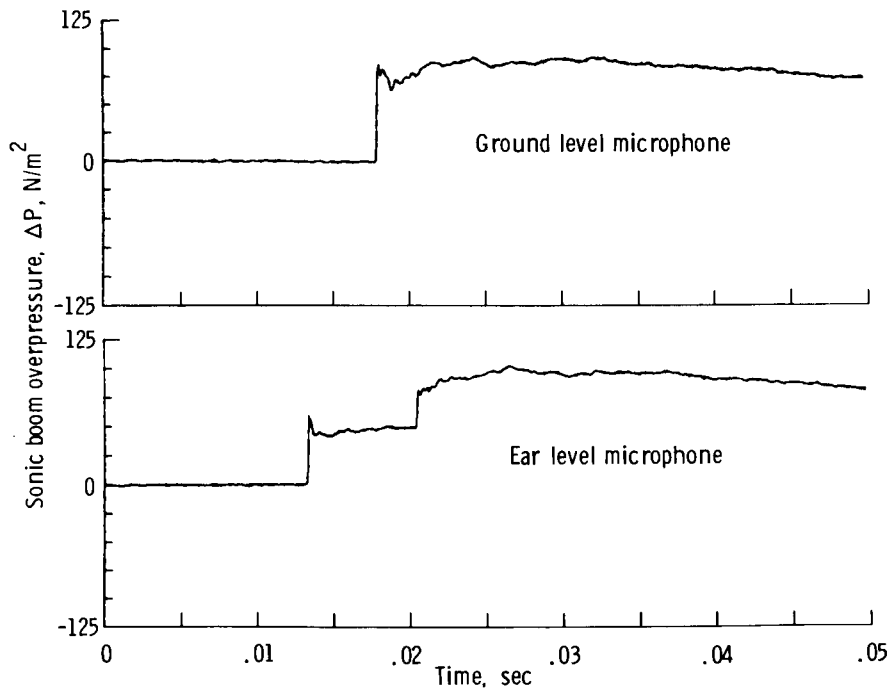
(h) Station 7.

Figure 11.- Continued.
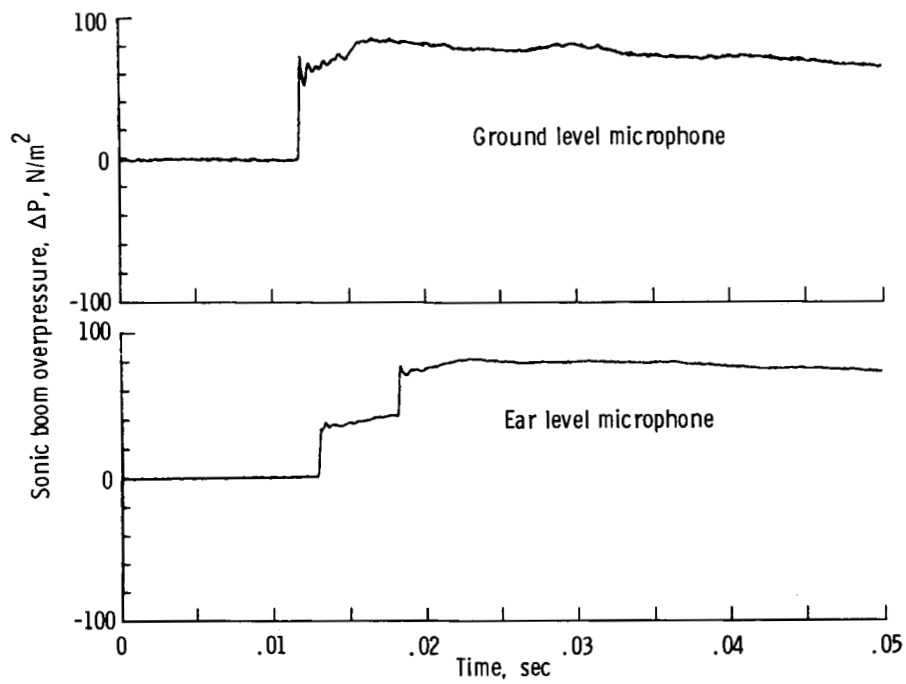
(i)　Station 8.

Figure 11.- Continued.
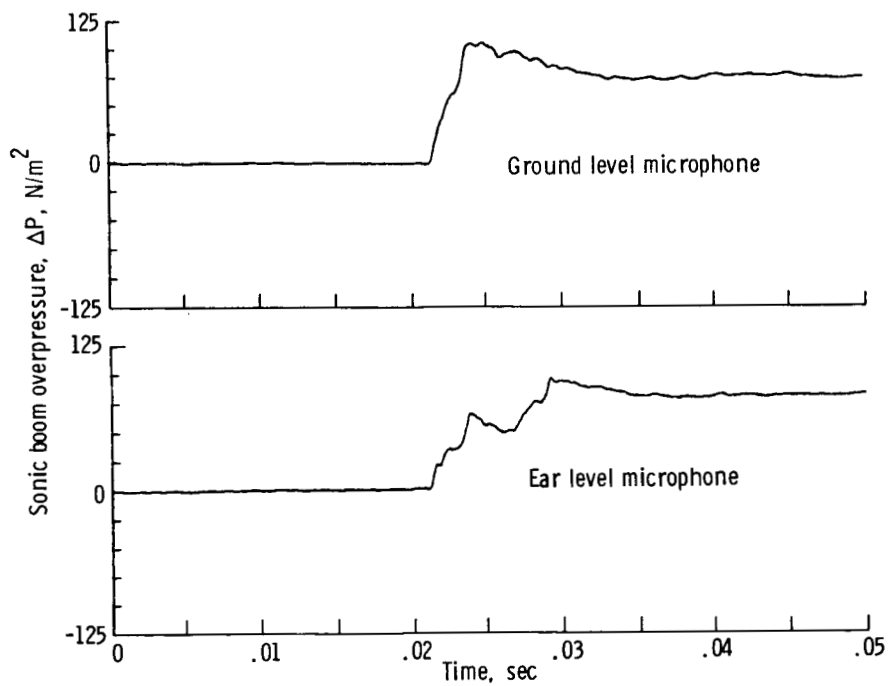
(j)　Station 9.

Figure 11.- Continued.
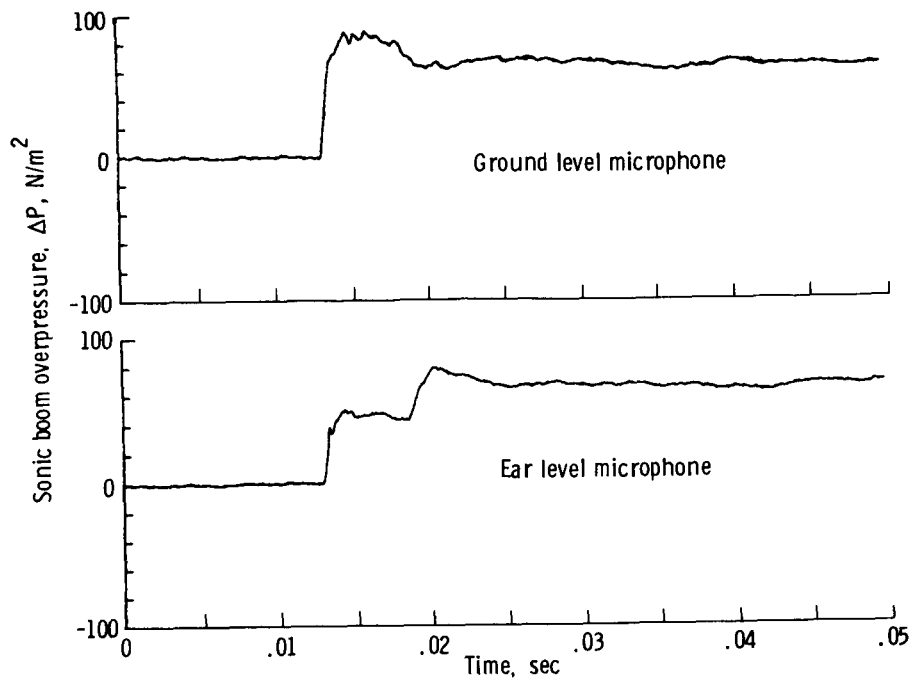
(k)   Station 10.

Figure 11.- Concluded.
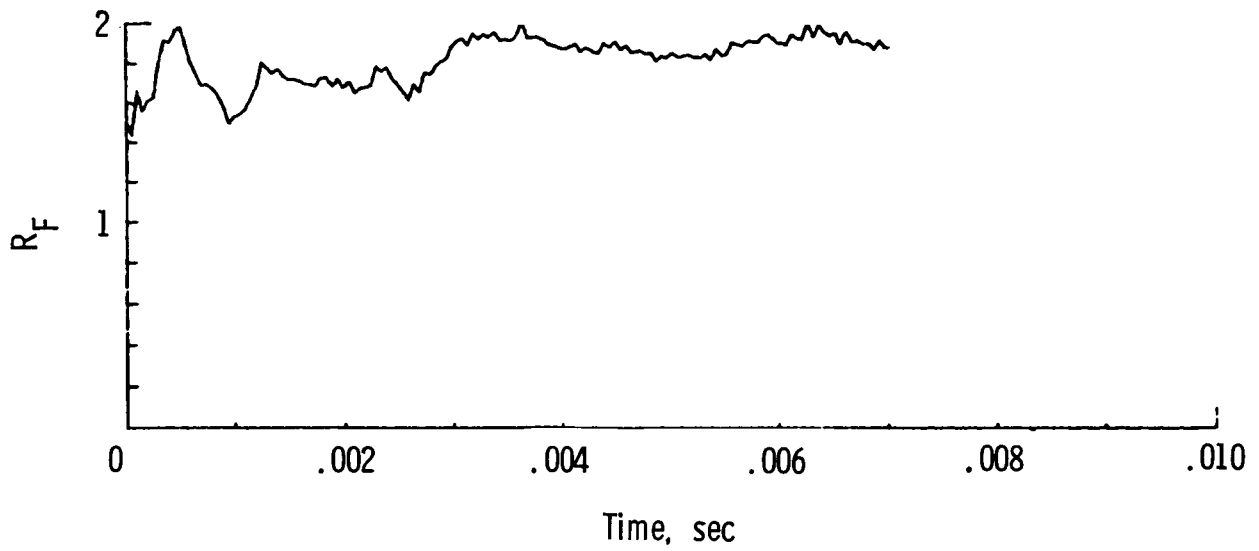
(a) Station 7.

Figure 12.- Typical reflection factor time histories of sonic boom signatures.
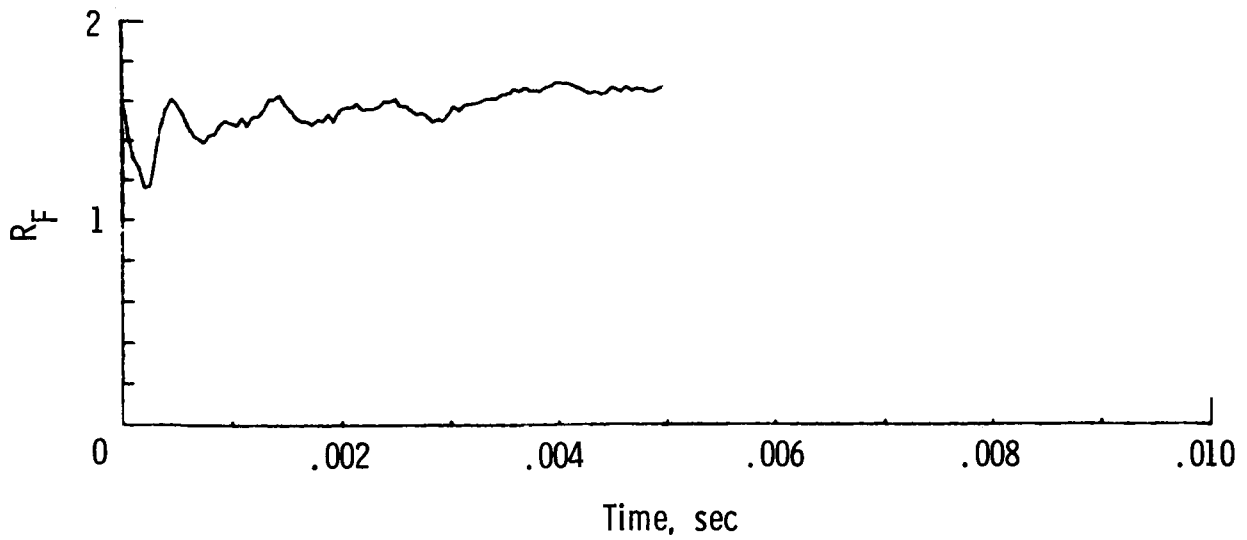
(b) Station 8.

Figure 12.- Concluded.
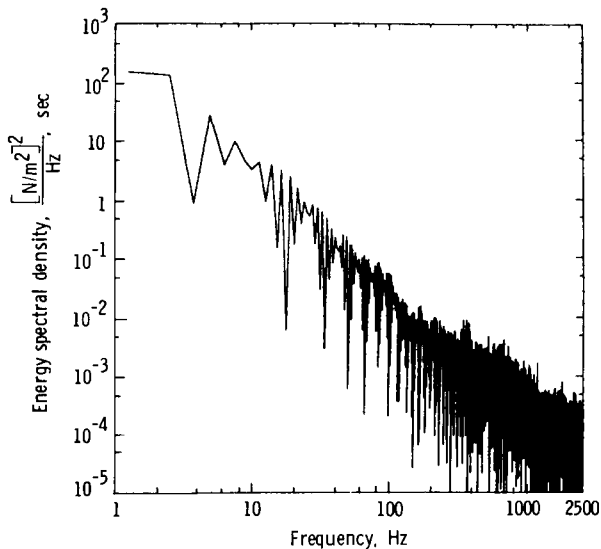
(a) Station 7 ground level microphone.

Figure 13.- Reentry energy spectral density.
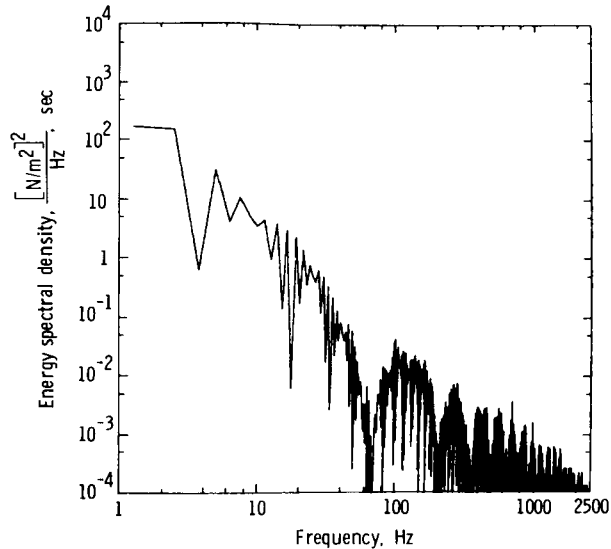
(b) Station 7 ear level microphone.

Figure 13.- Continued.
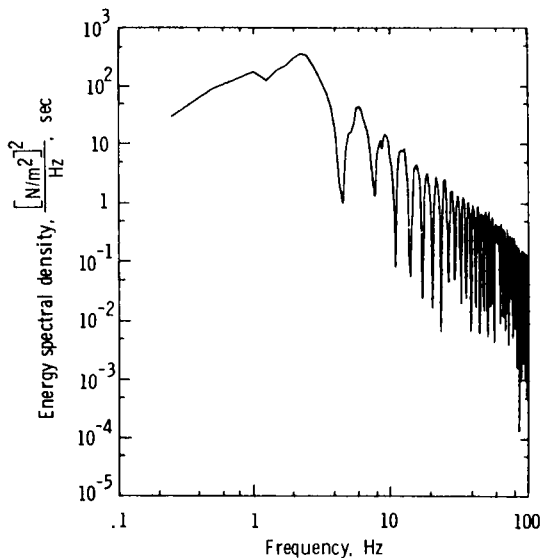
(c) Station 9 ground level microphone.

Figure 13.- Continued.
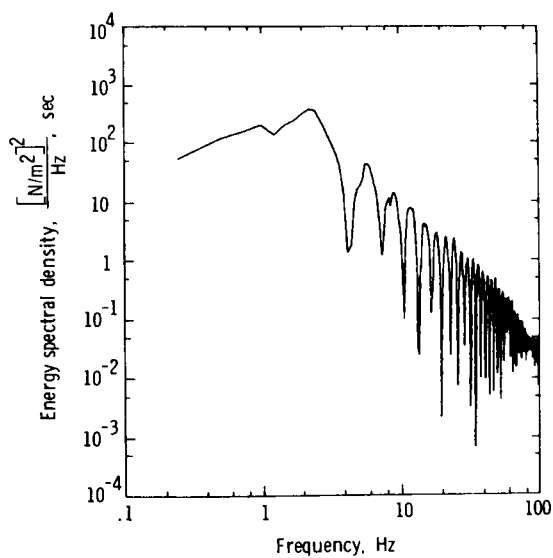
(d) Station 9 ear level microphone.

Figure 13.- Concluded.
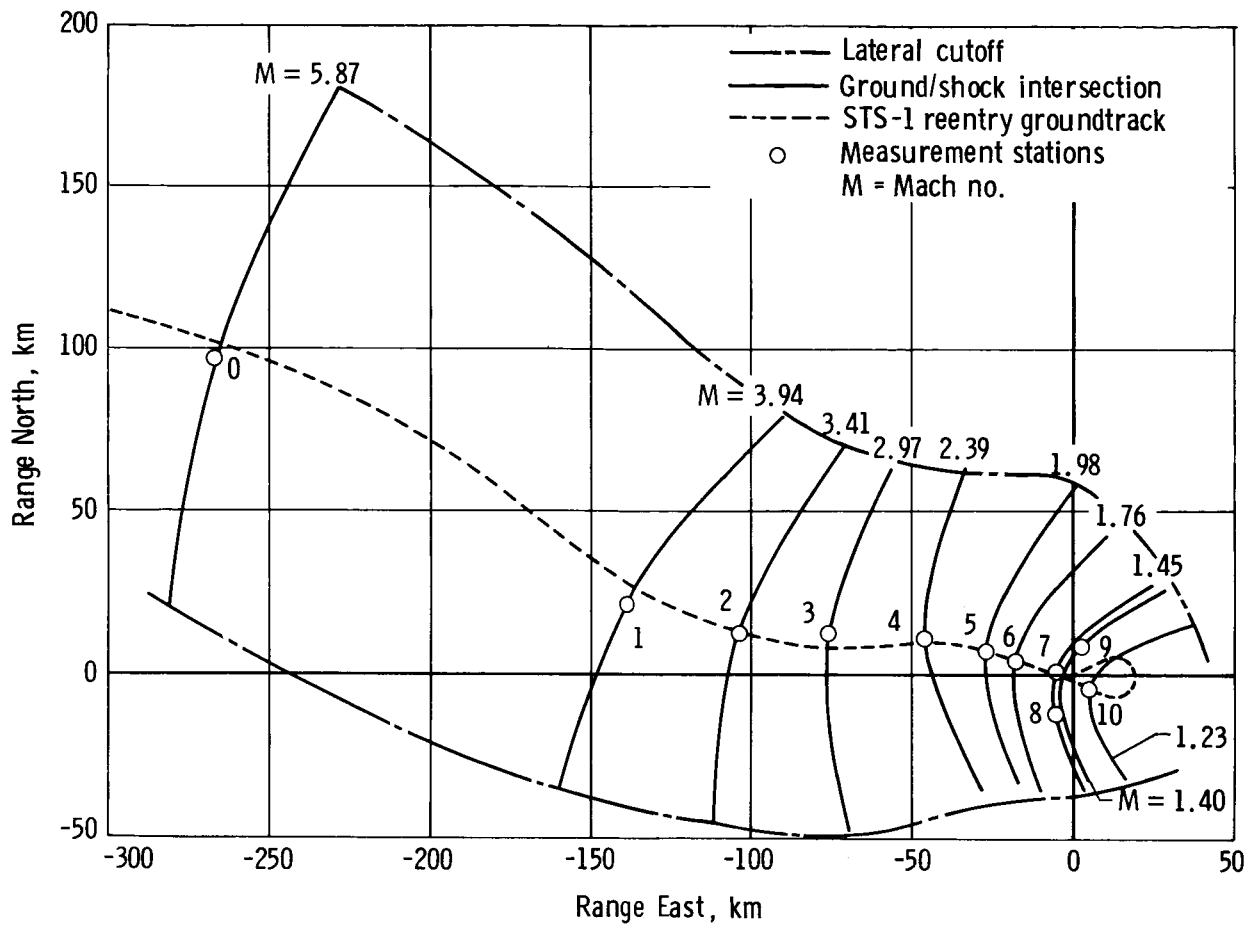
Figure 14.- Reentry shock/ground intersections through station locations.
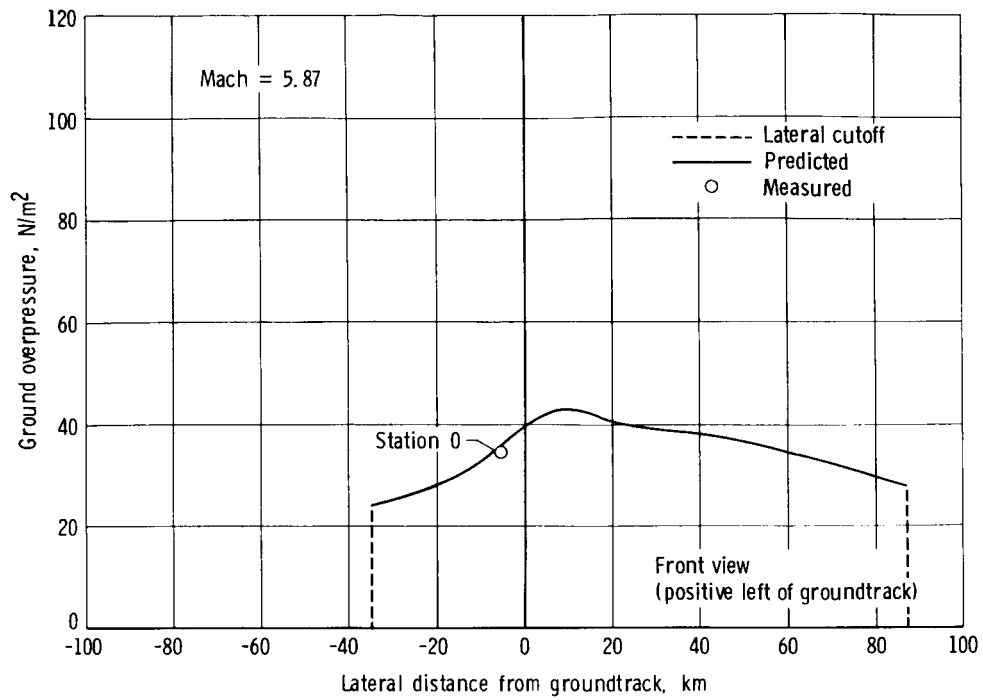
(a) Station 0.

Figure 15.- Lateral distribution of reentry overpressures along shock/ ground intersections.
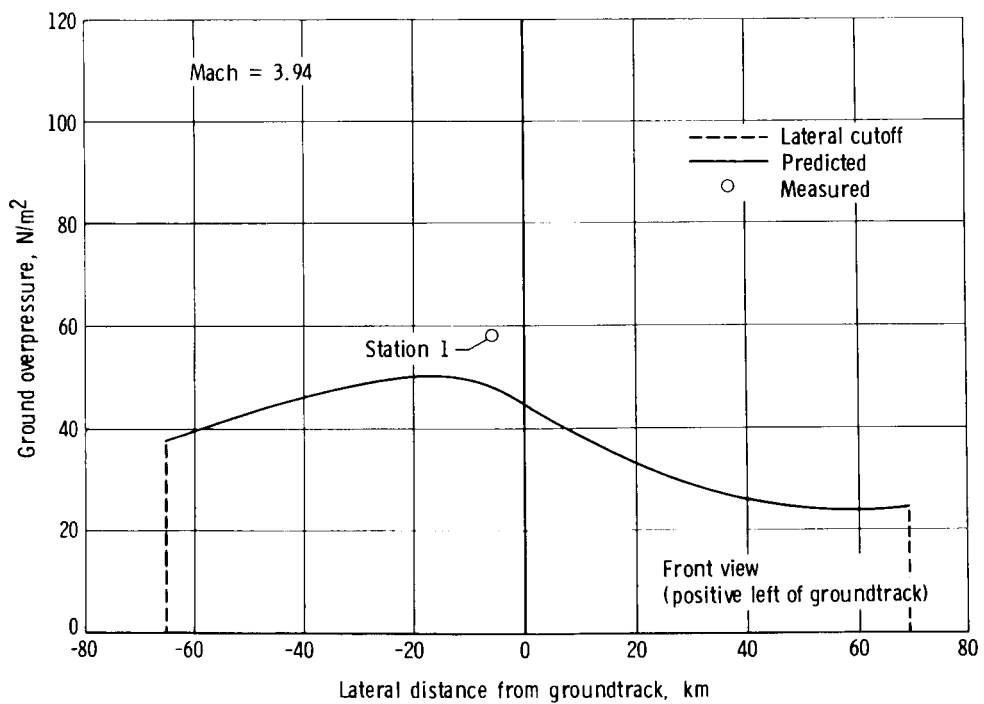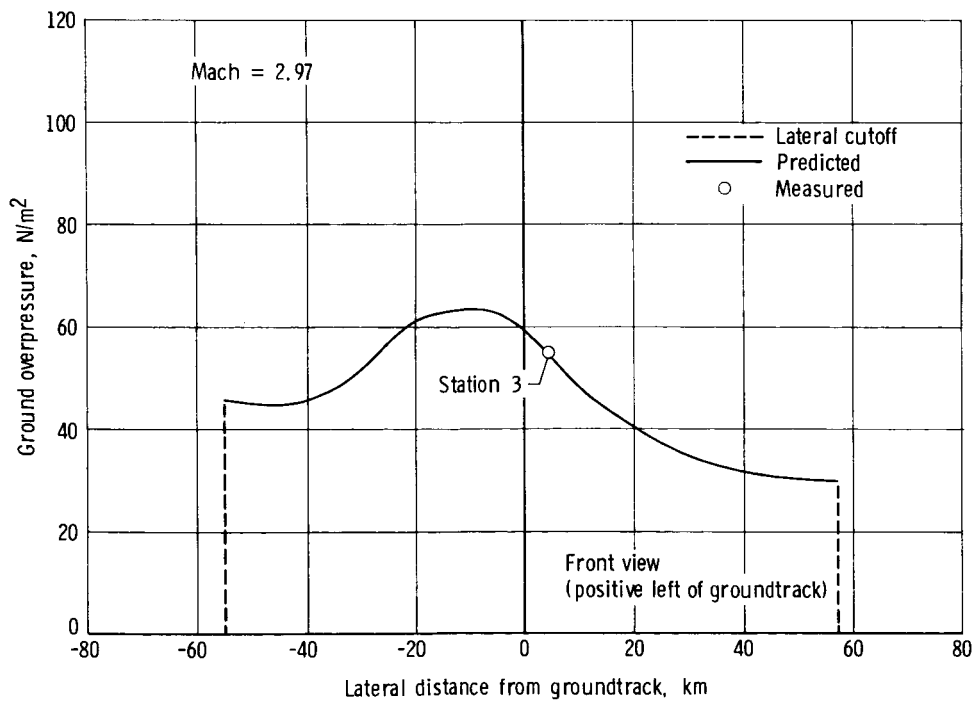

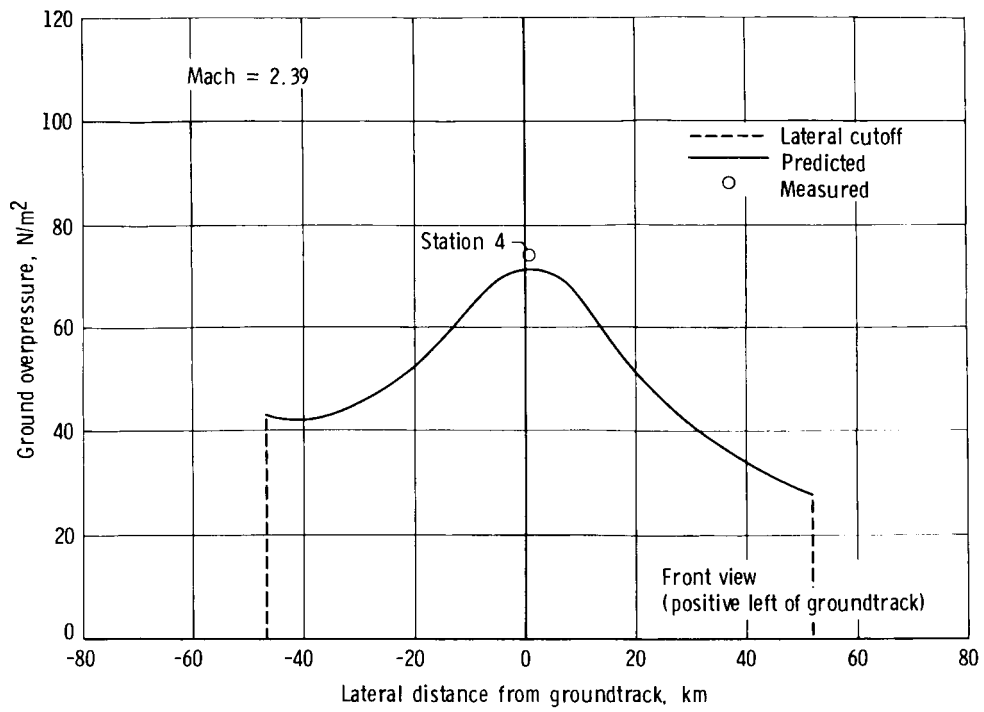(b) Station 1.

Figure 15.- Continued.
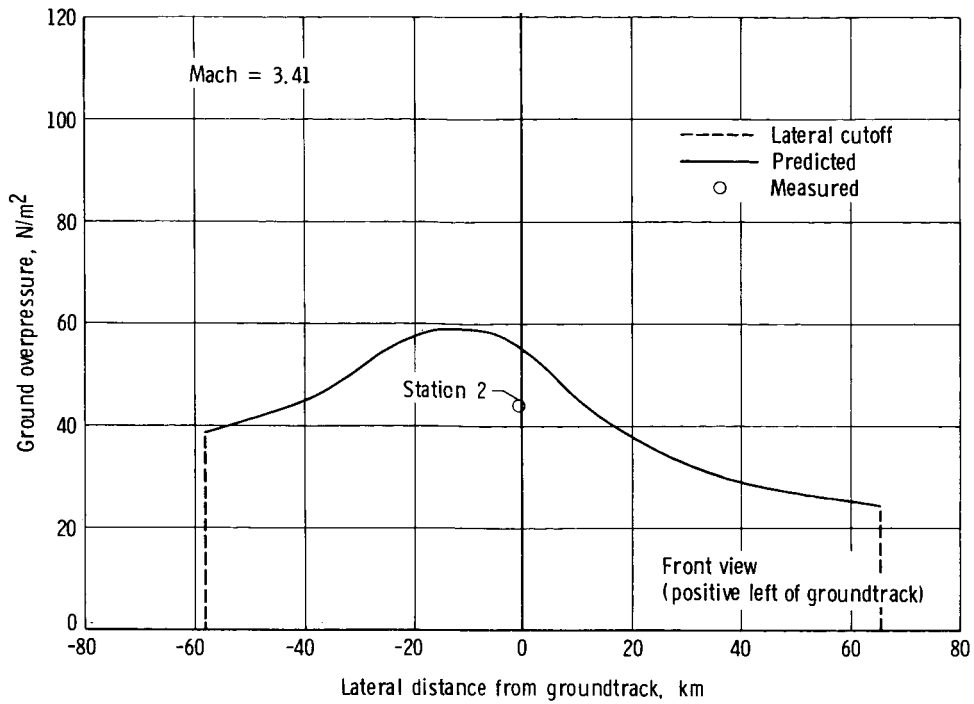
(c) Station 2.

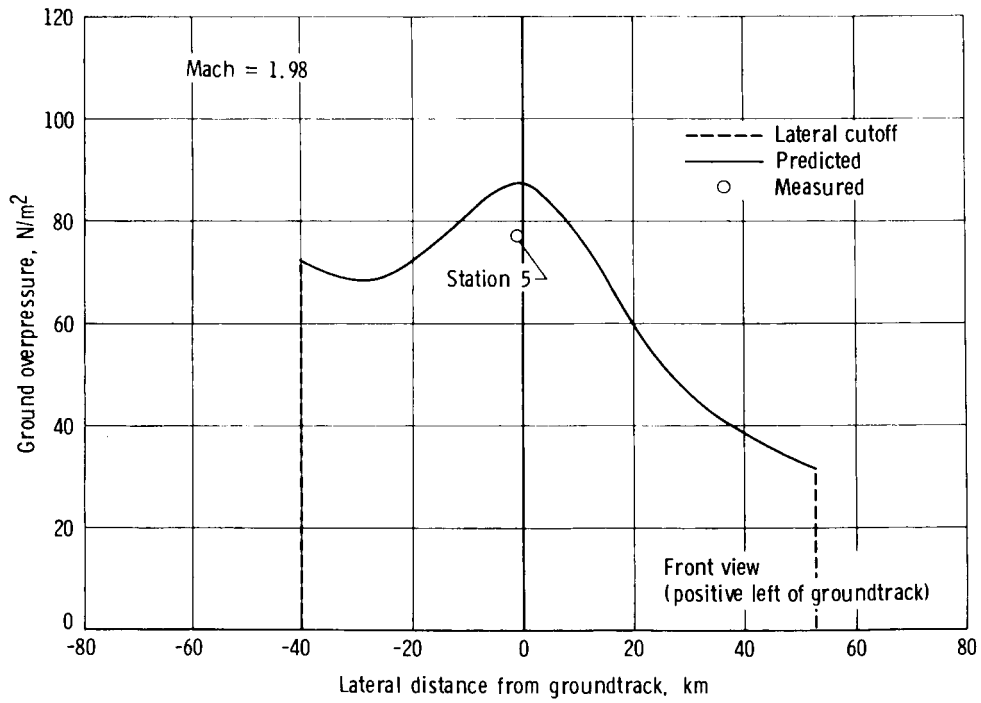Figure 15.- Continued.

(d) Station 3.
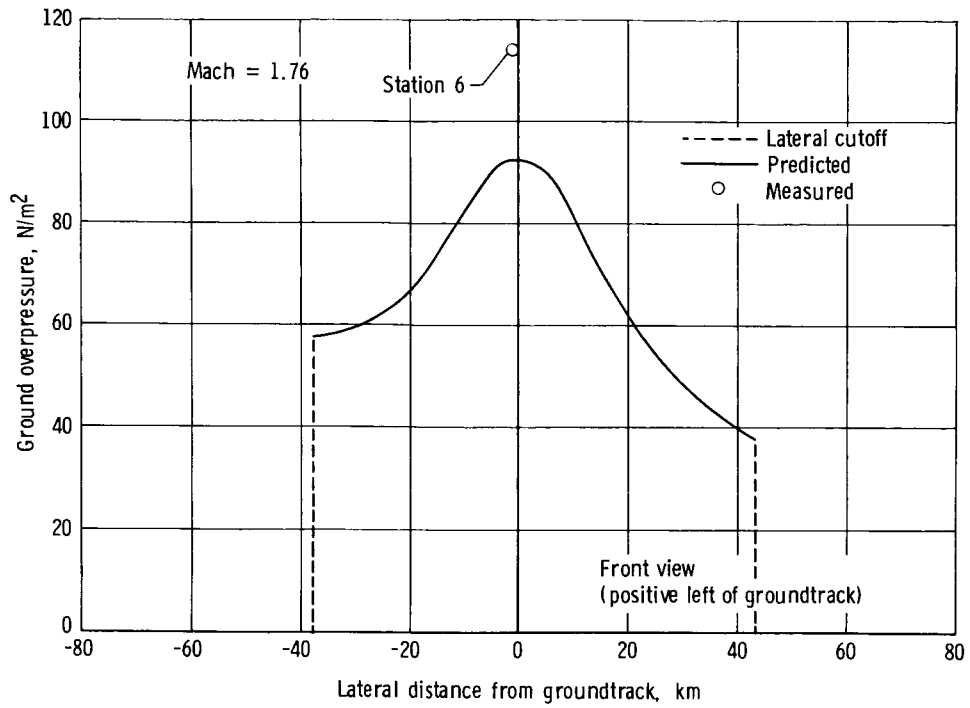
Figure 15.- Continued.

(e)   Station 4.
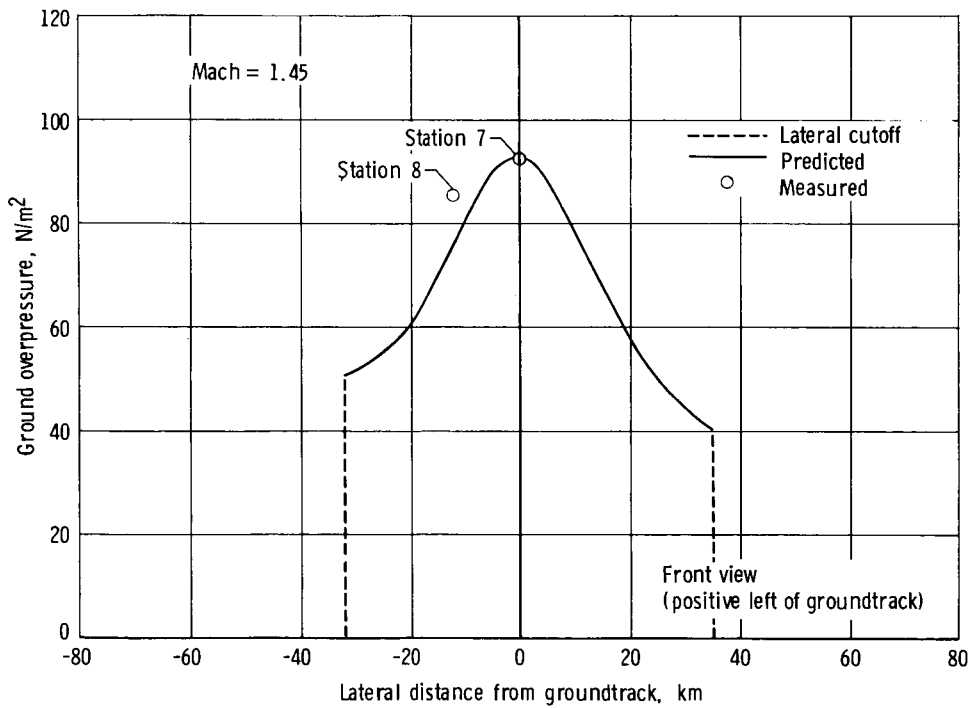
Figure 15.- Continued.

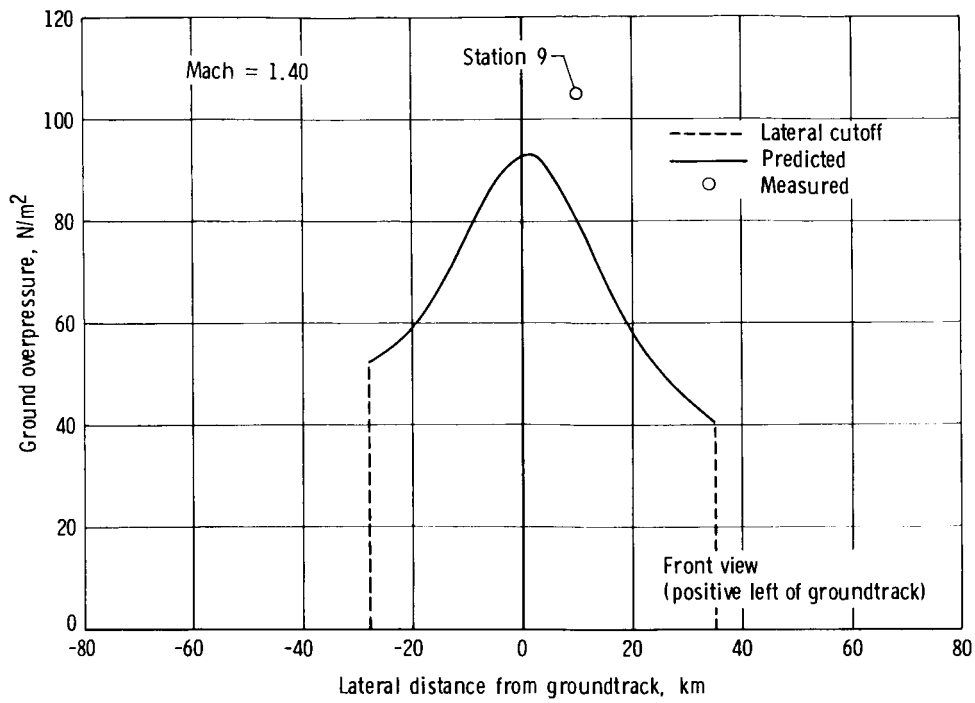(f)   Station 5.

Figure 15.- Continued.

(g) Station 6.

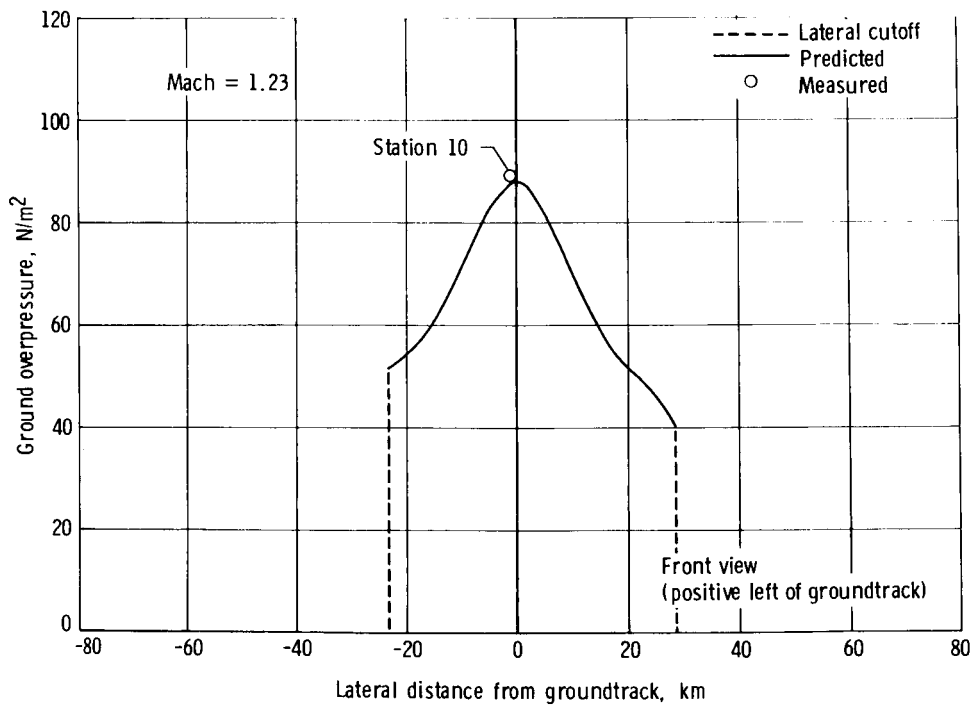Figure 15.- Continued.

(h) Stations 7 and 8.

Figure 15.- Continued.

(i)   Station 9.

Figure 15.- Continued.

(j)   Station 10.

Figure 15.- Concluded.

1. Report No. NASA TP-2475	2. Government Accession No.	3. Recipient's Catalog No.
4. Title and Subtitle CORRELATION OF PREDICTED AND MEASURED SONIC BOOM CHARACTER- ISTICS FROM THE REENTRY OF STS-1 ORBITER		5. Report Date June 1985
		6. Performing Organization Code 953-36-00-00-72
7. Author(s) Frank Garcia, Jr., Jess H. Jones, and Herbert R. Henderson		8. Performing Organization Report No. S-544
		10. Work Unit No.
9. Performing Organization Name and Address Lyndon B. Johnson Space Center Houston, Texas 77058		11. Contract or Grant No.
		13. Type of Report and Period Covered Technical Paper
12. Sponsoring Agency Name and Address National Aeronautics and Space Administration Washington, D.C. 20546		14. Sponsoring Agency Code

15. Supplementary Notes

Frank Garcia, Jr., Lyndon B. Johnson Space Center
Jess H. Jones, Marshall Space Flight Center
Herbert R. Henderson, Langley Research Center

16. Abstract

Characteristics from sonic boom pressure signatures recorded at 11 locations during reentry of the Space Shuttle Orbiter Columbia are correlated with characteristics of wind tunnel signatures extrapolated from flight altitudes for Mach numbers ranging from 1.23 to 5.87. The flight pressure signatures were recorded by microphones positioned at two levels near the descent groundtrack along the California corridor. The wind tunnel signatures used in theoretical predictions were measured using a 0.0041-scale model Orbiter. The mean difference between all measured and predicted overpressures is 12 percent from measured levels. With one exception, the flight signatures are very similar to theoretical N-waves.

17. Key Words (Suggested by Author(s)) Supersonic aircraft Aerodynamic character- istics Acoustic measurements Shock waves Theoretical N-waves Energy spectral density Fourier analysis Reflection factor Wind tunnel measure- ments	18. Distribution Statement Unclassified – Unlimited Subject Categories 71, 02
19. Security Classif. (of this report) Unclassified	20. Security Classif. (of this page) Unclassified 21. No. of Pages 49 22. Price A03

JSC Form 1424 (Rev Nov 75)

NASA-Langley, 1985

National Aeronautics and
Space Administration

Washington, D.C.
20546

Official Business
Penalty for Private Use, $300

NASA